

A Systematic Benchmark Study of Free Energy Methods for Quantifying Light-Responsive Binding Affinities of Photoswitchable Antagonists of Beta-Adrenergic Receptors

Mohammad Khavani, Amirhossein Bakhtiari, Laleh Khalvati, Rob Leurs, and Ruibin Liang*

Cite This: <https://doi.org/10.1021/acs.jmedchem.5c03756>

Read Online

ACCESS |



Metrics & More

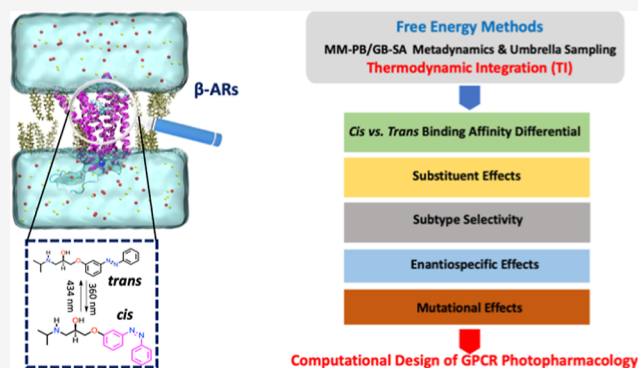


Article Recommendations



Supporting Information

ABSTRACT: Molecular photoswitches enable spatiotemporal photocontrol of protein function, but their design requires high target selectivity and large light-dependent changes in binding affinity and/or efficacy. These properties are especially difficult to optimize in membrane receptors due to membrane–protein interactions. Computational design remains challenging because few benchmarks rigorously compare free-energy methods against experiment. Here, we establish such a benchmark for photoswitchable antagonists of β -adrenergic receptors, exemplifying most successful designs in the photopharmacology of class A G protein-coupled receptors (GPCRs) to date. We evaluated widely used free-energy methods for predicting how substituents and chirality affect light-responsive binding and subtype selectivity. Thermodynamic integration shows the best agreement with experiment, followed by umbrella sampling, whereas metadynamics and end-point methods perform poorly. Our simulations reveal interactions stabilizing *cis* OP2 in β_2 -AR and the key role of PHE289 in isomer-specific binding, consistent with mutagenesis data. Overall, this work provides a robust computational framework for GPCR photopharmacology.



INTRODUCTION

Molecular photoswitches enable the remote, reversible, and precise manipulation of biological processes via light, offering potential candidates for novel therapeutics with minimal side effects in photopharmacology.^{1–6} They are designed to isomerize bidirectionally when exposed to different wavelengths of light, and thermally relax to the most energetically stable isomer form in the dark-adapted state. Usually, one isomeric form mimics the structure of a parent non-photochromic compound, which is an agonist or antagonist targeting a specific biomolecular target (e.g., a membrane receptor), while the other isomeric form differs significantly from the parent compound. Thus, the photoinduced and thermally driven isomerization of the photoswitches alters their binding affinity and/or efficacies toward the biomolecular target. Moreover, their photochemical properties and protein–ligand interactions can be fine-tuned through careful design and organic synthesis, enabling precise and reversible photocontrol of various targeted biological processes.^{1–6} This makes them promising candidates for the photopharmacology of various diseases, such as cardiovascular diseases,^{5,7} neurodegenerative disorders,^{8,9} cancer,¹⁰ and vision loss.¹¹

Designing effective photoswitchable ligands usually relies on maximizing the difference in the binding affinities and/or efficacies between the active and inactive isomeric forms

toward a specific biomolecular target. This maximizes light-responsiveness of bioactivity while minimizing cytotoxicity outside illuminated regions, thereby fulfilling the goal of precise photocontrol of the drug activity. Therefore, to design photoswitchable drugs, it is critical to predict how chemical modifications influence (1) absolute binding affinity toward a specific target, (2) difference in the binding affinity and/or efficacies between distinct isomers toward this target, which affects the precision of photocontrol, and (3) binding selectivity between proteins in distinct subclasses within the same superfamily, which minimizes off-target effects.

Achieving all three goals experimentally often involves tedious trials and errors, and molecular simulations can be a useful tool in their rational design. However, major challenges exist because prediction errors as small as a few kcal/mol in the binding affinity difference between distinct isomers can lead to a qualitatively incorrect identification of the active isomer, thereby greatly hindering design efforts. For example, a “*cis*-on”

Received: December 19, 2025

Revised: March 9, 2026

Accepted: April 1, 2026

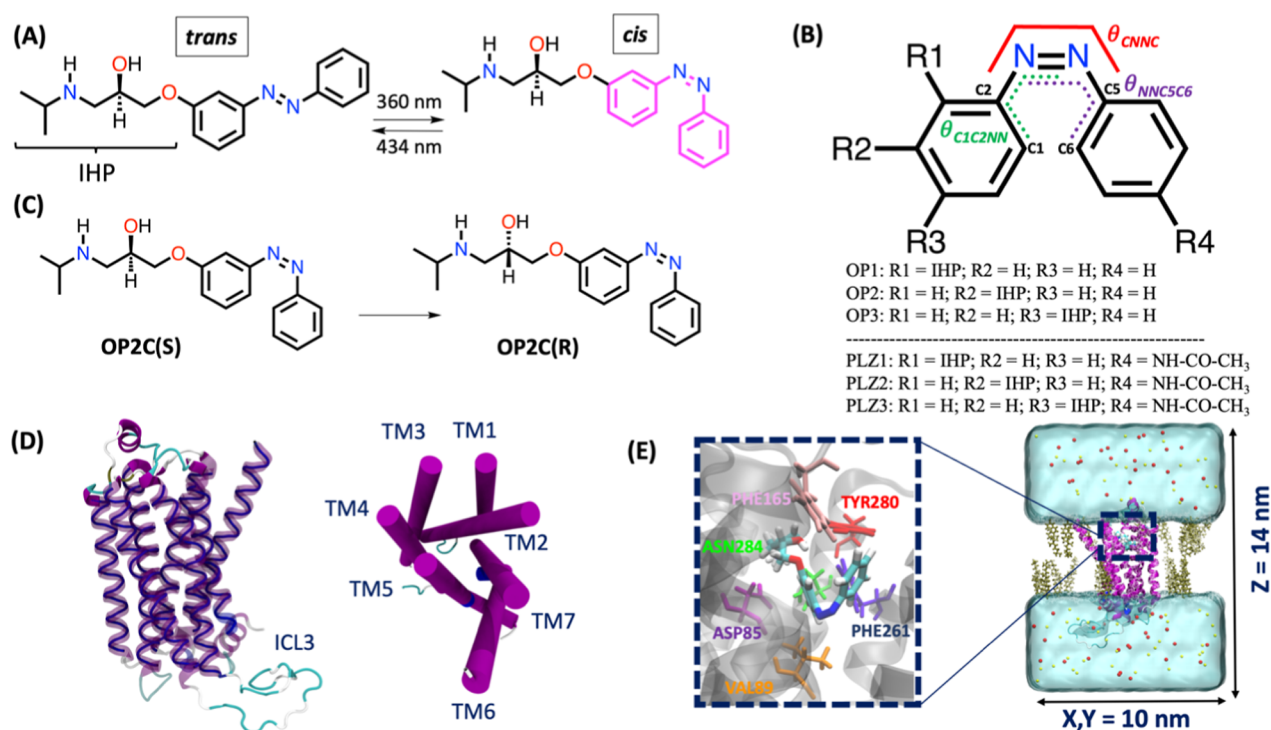


Figure 1. (A) The bidirectional photoisomerization of opto-prop-2 (OP2) under illumination of different wavelengths. (B) The chemical structures of OPs and PLZs with different R-group substitutions. The drug's side chain is 3-(isopropylamino)-2-hydroxypropoxy, abbreviated as IHP. For each pair of PLZ and OP with the same index, e.g., the PLZ1 and OP1, the IHP side chain is located at the same position (ortho, meta, or para) on the azobenzene moiety. (C) A schematic representation of the conversion from the S-enantiomer of the *cis* OP2 (OP2C(S)) to its R-enantiomer (OP2C(R)). (D) The structure of β_2 -AR, shown from side and top-down views, with the intracellular loop (ICL3) highlighted. The structure of the β_1 -AR is presented in Figure S2. (E) Simulation setup of β_2 -AR embedded in a DOPC/cholesterol mixed lipid bilayer, showing the binding pocket with highlighted residues that interact with the ligand (OP2 as an example). Cholesterol, Na⁺, and Cl⁻ ions are shown in tan, red, and yellow colors, respectively. For clarity, the DOPC units and water molecules are displayed transparently.

azobenzene-based ligand exhibits higher affinity in the *cis* isomer than the *trans* isomer, and its activity is turned on by light because the dark-adapted state is dominated by the thermally more stable but inactive *trans* isomer. In contrast, a “*trans*-on” azobenzene ligand is active in the dark-adapted state (*trans* isomer), which is turned off by light (*cis* isomer). On top of this challenge, predicting how substituents affect the light-responsive difference in binding affinity between distinct isomers (referred to as “light-responsive affinity differential” below) is even more difficult, where intuitions often fail.^{4,12} Moreover, it is especially challenging to predict ligand binding affinities in membrane proteins due to the conformational fluctuations arising from the dynamic interplay of protein–membrane and protein–ligand interactions,¹³ which have nontrivial effects on the ligand binding process and the associated allosteric effects within the protein.

Conventional methods fail almost completely to address these challenges. For example, it has been shown that docking and unbiased molecular dynamics (MD) simulations are inaccurate even for qualitatively estimating the effects of substituents on the light-responsive affinity differential.^{4,14,15} Only a few studies have used free energy calculations to quantify light-responsive affinity differential of small-molecule drugs,^{16–18} and there has been a lack of systematic benchmarking of the accuracy of free energy methods for predicting the effects of substituents on these quantities against experimental data.

To bridge this gap, here, for the first time, we systematically benchmarked several popular free energy methods against

experiments to quantify how substituents affect (1) the absolute binding affinity, (2) light-responsive affinity differential, and (3) binding affinity preferences toward the target protein against other subtypes in the same family. These methods include the Thermodynamic Integration (TI),^{19–21} Umbrella Sampling (US),^{22–24} Metadynamics,^{25–28} and Molecular Mechanics Poisson–Boltzmann/Generalized-Born Surface Area (MM-PB/GB-SA).^{29,30} They were tested on a series of photoswitchable antagonists^{7,31,32} targeting beta-adrenergic receptors (β -ARs), which belong to the class A G-protein-coupled receptor family. GPCRs are one of the largest families of membrane receptors and have been intensively targeted for the treatment of various diseases.³³ In recent years, the photopharmacology of GPCRs, pioneered by one of us, has undergone rapid development, enabling photocontrol of cell signaling processes.^{5,7,31,32,34–41} Among class A GPCRs, human β -ARs are widely studied therapeutic targets for treating cardiovascular and respiratory diseases.^{1,5,34,38–40,42–47} Therefore, designing photoswitchable ligands for β -ARs can open new doors to precisely control a diverse set of biomedically relevant signaling pathways^{48–53} using light.

The photoswitches we investigated here were recently developed experimentally as light-regulated analogs of propranolol,^{7,31,32} a hallmark beta-blocker that antagonizes the β_1 -AR and β_2 -AR, and treats cardiovascular diseases. Replacing the naphthalene group of propranolol with an azobenzene moiety produced three photoswitchable analogs: opto-prop-1 (OP1), opto-prop-2 (OP2), and opto-prop-3 (OP3)^{7,32} (Figure 1 A & B), which were designed in our

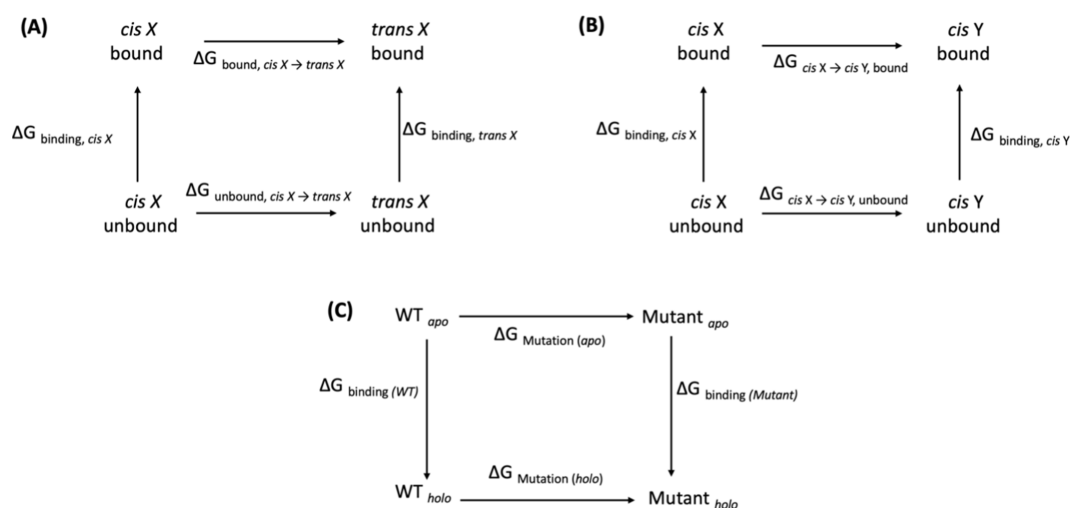


Figure 2. Thermodynamic cycles for calculating the light-responsive affinity differential and the effects of substituents and mutations. (A) In Approach A, each compound X is alchemically transformed from the *cis* isomer into its *trans* isomer. The TI simulation estimates the free energy change of this process in both protein ($\Delta G_{\text{bound, cis X} \rightarrow \text{trans X}}$) and solution ($\Delta G_{\text{unbound, cis X} \rightarrow \text{trans X}}$). The cycle is employed to estimate the relative binding free energy between the *cis* and *trans* isomers, i.e., the *cis*-vs-*trans* affinity differential ($\Delta \Delta G_{\text{X, cis} \rightarrow \text{trans}}$) using eq 1. (B) In Approach B, compound X is alchemically transformed into Y in the same isomeric form (Approach B). The TI simulation estimates the free energy change of this process in both protein ($\Delta G_{\text{cis X} \rightarrow \text{cis Y, bound}}$) and aqueous solution ($\Delta G_{\text{cis X} \rightarrow \text{cis Y, unbound}}$). The cycle is employed to estimate the relative binding affinity between X and Y ($\Delta \Delta G_{\text{binding, cis X} \rightarrow \text{cis Y}}$, $\Delta \Delta G_{\text{binding, trans X} \rightarrow \text{trans Y}}$) using eqs 2 and 3. Based on the two relative binding free energies calculated in either approach, the effect of transforming X to Y on the *cis*-vs-*trans* affinity differential was calculated using eq 4. (C) Thermodynamic cycle for estimating the effect of mutating PHE289 residue to Ala (F289A) on the binding affinities of *cis* and *trans* isomers of OP2 in complex with β_2 -AR. The relative binding affinities between wild type (WT) and Mutant (Mut) of β_2 -AR ($\Delta \Delta G_{\text{binding, cis (WT)} \rightarrow \text{cis (Mut)}}$ and $\Delta \Delta G_{\text{binding, trans (WT)} \rightarrow \text{trans (Mut)}}$) were calculated using eqs 6 & 7.

previous experimental studies.^{7,32} They have varying binding affinities and light-responsive affinity differential in β_1 -AR and β_2 -AR.^{7,31,32} For all three compounds, the *trans* isomer is thermally more stable than the *cis* isomer in the ground electronic state. The OP2 exhibits the highest light-responsive affinity differential for β_2 -AR, with its *cis* isomer being the functionally active state. This compound is among one of the most successful candidates for the photopharmacology of class A GPCRs. The three OPs also exhibit different binding selectivity between the β_1 -AR and β_2 -AR. The “*cis*-on” effect of OP2 in β_2 -AR is also enantiospecific, with OP2(S) featuring a greater effect than OP2(R)³² (Figure 1C), highlighting the role of chirality in fine-tuning light-responsive affinity differential.^{7,32} Furthermore, Photoazolo (PLZ) is another recently developed series of photoswitchable propranolol analogs, exhibiting considerable antagonist activity for β_2 -AR.³¹ Compared to OPs, PLZs only have one additional *p*-acetamido group (Figure 1A,B), but this small modification leads to key differences in light-responsive affinity differential.³¹ For example, OP2 shows a 587-fold increase in binding affinity toward β_2 -AR upon switching from the *trans* to *cis* isomer, whereas PLZ2 greatly reduces this light-responsive affinity differential to just 3.6-fold. Thus, computationally studying the OP and PLZ series can reveal how small chemical modifications on the photoswitch affect light-responsive bioactivity of β -AR antagonists.

Our results indicate that substituents and chirality strongly affect light-responsive affinity differential and subtype selectivity between β_1 -AR and β_2 -AR, and that Thermodynamic Integration (TI) provides the most reliable predictions consistent with experiments. Other methods, such as US, Well-Tempered Metadynamics (WT-MTD), and MM/PBSA (GBSA), exhibit significant discrepancies with the experiment.

Additionally, the MD simulation offers valuable atomic-level insights into the strengths and limitations of current modeling techniques for light-responsive ligand–receptor interactions. These findings bridge the available experimental data and free energy calculations, and will advance the rational design of photoswitchable β -AR antagonists with enhanced light-responsiveness and subtype specificity.

COMPUTATIONAL METHODS

Here, we first introduce the system setup and equilibration simulations. Then, we detail the free energy methods including the TI, US, WT-MTD and MM/PBSA and MM/GBSA. eqs 1–8 and the thermodynamic cycles in Figure 2 are used for calculating various free energy quantities reported in the Results section.

System Setup and MD Equilibration Simulations

The crystal structure of the inactive β_2 -AR bound to propranolol (PDB ID: 6PSS)⁵⁴ was used as the starting structure for setting up the β_2 -AR simulations. Following the approaches of previous studies,⁵⁵ the T4-lysozyme (T4L) segment fused with the β_2 -AR in the crystal structure was removed. The intracellular loop (ICL3) of β_2 -AR missing from the crystal structure was reconstructed as an unstructured loop using the MODELLER⁵⁶ software package (Figure 1D). The mutated residues in the crystal structure were modified back to the wild-type sequence using the same package. The propranolol ligand was removed, and molecular docking simulations were performed using AutoDock Vina software⁵⁷ to place a single molecule of OP or PLZ in the binding pocket in either the *cis* or *trans* isomer. The structure of the docked ligand was visually checked such that the azobenzene moiety has maximal overlap with the hydrophobic ring of the original ligand (propranolol), and cross-compared with those in ref 32 whenever possible. The protonation states of the ionizable residues at neutral pH were determined using the H++ server.⁵⁸ The CHARMM-GUI server⁵⁹ was utilized for embedding the β_2 -AR and β_1 -AR in a lipid bilayer, which is capped on both sides by boxes of water molecules with 40 Å thickness. In all setups, the membrane was

composed of 180 molecules of DOPC (1,2-dioleoyl-*sn*-glycero-3-phosphocholine) combined with 10 wt % cholesterol. This specific DOPC/cholesterol ratio was selected based on prior studies that examined how cholesterol concentration influences the stability and dynamic properties of the receptor within the lipid bilayer.^{60,61} To mimic physiological conditions, 0.15 M NaCl was added, which also neutralized the net charge of the system (Figure 1E). The resulting periodic boundary condition (PBC) simulation box has a dimension of $\sim 100 \times 100 \times 140 \text{ \AA}^3$. For the β_1 -AR simulation setups, the crystal structure of β_1 -AR bound to the carazolol ligand (PDB ID: 7BVQ)⁶² was used, and a similar setup procedure was followed.

The TIP3P model was employed to treat the water molecules,⁶³ while the FF14SB⁶⁴ and LIPID17⁶⁵ force fields were employed to treat the proteins and the lipid bilayer, respectively. The general AMBER Force Field (GAFF) approach^{66,67} was employed to parametrize the force fields of the ligands (OP1, OP2, OP3, PLZ1, PLZ2, and PLZ3). The torsional terms associated with three key dihedrals in the azobenzene moiety, i.e., the C2–N3=N4–C5 (θ_{CNNC}), C1–C2–N3=N4 (θ_{C1C2NN}), and N3=N4–C5–C6 (θ_{NNC5C6}) (Figure 1B), were parametrized based on the relaxed scans of the potential energy surface (PES) along these coordinates using a quantum mechanical (QM) method. This procedure is necessary because our previous study⁶⁸ has shown that utilizing the GAFF parameters for these torsions without modification usually leads to structural distortions from the expected planar geometry in the *trans* isomer during MD simulations. Consequently, careful refinement of these dihedral parameters was necessary for accurate free energy calculations. To this end, the hh-TDA-DFT method⁶⁹ with the BH&HLYP functional and 6-311++G(d,p) basis set was employed as the QM method. This multireference QM method has been well benchmarked for studying photochemical reactions of azobenzene-derived photoswitches,^{68–72} and the use of the multi-reference QM method was demonstrated to be important for describing the transition state of ground-state isomerization.⁷³ The torsional parameters were fine-tuned such that the molecular mechanics (MM) PES reproduced the QM PES regarding the *cis*-to-*trans* isomerization barrier heights and the energy differences between the two isomers (Figure S1). All QM calculations in the force field parametrization were performed with the TeraChem software package.^{74,75}

The systems were first subject to 100,000 steps of energy minimization. Following this, the system was equilibrated in the constant *NVT* ensemble at 300 K for 5 ns, with a time step of 1 fs. During this step, harmonic biasing potentials with force constants of $5.0 \text{ kcal}\cdot\text{mol}^{-1}\cdot\text{\AA}^{-2}$ were imposed on all protein heavy molecules. Then, the systems were equilibrated for 50 ns in the constant *NPT* ensemble (300 K, 1 bar) with a 1 fs time step, during which the protein restraints were gradually reduced to zero. In the final step, production MD simulations were conducted for 1.1 μs in the same constant *NPT* ensemble with a 2 fs time step, with no protein restraints. The pressure was controlled using the anisotropic Berendsen method⁷⁶ with a relaxation time of 1 ps. Temperature control was achieved through the Langevin thermostat⁷⁷ with a friction coefficient of 1 ps^{-1} . Long-range electrostatic interactions were treated using the Particle Mesh Ewald (PME)⁷⁸ method, and a 12 \AA cutoff was applied for the van der Waals interactions. Additionally, all covalent bonds involving hydrogen atoms were constrained using the SHAKE algorithm throughout the simulations.⁷⁹ All geometry optimizations and MD simulations were performed using the AMBER24 software package.⁸⁰

It is worth noting that unbiased MD trajectories were used to analyze ligand–receptor interactions and characterize binding interaction profiles. The TI simulations generate trajectories from mixed Hamiltonians of the two end states. Thus, they represent intermediate states during alchemical transformations, and do not correspond to physically meaningful states, nor are they suited for analyzing interaction frequencies or per-residue contributions. For this reason, the molecular interaction analysis was performed using the unbiased production MD trajectories, where the ligand–receptor complex is fully interacting and structurally stable. This approach

allows meaningful identification of residue–ligand contacts and interaction patterns.

Free Energy Calculations

The equations below used for free energy calculations are summarized. Equation 1 was used for the relative binding affinities between *cis* and *trans* isomers of the same compound X, i.e., the light-responsive affinity differential. Equations 2 and 3 were used for the relative binding affinities between the same isomer of compounds X and Y in the same receptor. Equation 4 was used for the substituents' effects on the light-responsive binding affinity differential in the same receptor. Equation 5 was used for substituents' effects on the subtype selectivity between the β_1 -AR and β_2 -AR. Equations 6 and 7 were used for the relative binding affinities between the wild-type (WT) and the mutant (Mut) for the same isomer of the same compound. Equation 8 was used for the receptor's mutational effects on the light-responsive affinity differential for the same compound.

Thermodynamic Integration (TI)

The TI methods were employed to evaluate (1) the difference in the binding affinity between the *cis* and *trans* isomers (referred to as “*cis*-vs-*trans* affinity differential” below) for each compound ($\Delta\Delta G_{X,cis \rightarrow trans}$, Approach A), (2) the relative binding affinity between a pair of compounds (X and Y) in the same isomeric form ($\Delta\Delta G_{\text{binding},cisX \rightarrow cisY}$ and $\Delta\Delta G_{\text{binding},transX \rightarrow transY}$, Approach B). The R and S enantiomers of the OP2 were treated as two compounds in Approach B, each with its own *cis* and *trans* isomers.

$$\begin{aligned} \Delta\Delta G_{X,cis \rightarrow trans} &= \Delta G_{\text{binding},transX} - \Delta G_{\text{binding},cisX} \\ &= \Delta G_{\text{bound},cisX \rightarrow transX} - \Delta G_{\text{unbound},cisX \rightarrow transX} \end{aligned} \quad (1)$$

$$\begin{aligned} \Delta\Delta G_{\text{binding},cisX \rightarrow cisY} &= \Delta G_{\text{binding},cisY} - \Delta G_{\text{binding},cisX} \\ &= \Delta G_{cisX \rightarrow cisY,\text{bound}} - \Delta G_{cisX \rightarrow cisY,\text{unbound}} \end{aligned} \quad (2)$$

$$\begin{aligned} \Delta\Delta G_{\text{binding},transX \rightarrow transY} &= \Delta G_{\text{binding},transY} - \Delta G_{\text{binding},transX} \\ &= \Delta G_{transX \rightarrow transY,\text{bound}} - \Delta G_{transX \rightarrow transY,\text{unbound}} \end{aligned} \quad (3)$$

$$\begin{aligned} \Delta\Delta\Delta G_{X \rightarrow Y,cis\text{-vs-}trans\text{ binding}} &= \Delta\Delta G_{Y,cis \rightarrow trans} - \Delta\Delta G_{X,cis \rightarrow trans} \\ &= [\Delta G_{\text{binding},transY} - \Delta G_{\text{binding},cisY}] \\ &\quad - [\Delta G_{\text{binding},transX} - \Delta G_{\text{binding},cisX}] \\ &= [\Delta G_{\text{binding},transY} - \Delta G_{\text{binding},transX}] \\ &\quad - [\Delta G_{\text{binding},cisY} - \Delta G_{\text{binding},cisX}] \\ &= \Delta\Delta G_{\text{binding},transX \rightarrow transY} - \Delta\Delta G_{\text{binding},cisX \rightarrow cisY} \end{aligned} \quad (4)$$

$$\begin{aligned} \Delta\Delta\Delta G_{cisX \rightarrow cisY,\beta_1\text{-AR vs } \beta_2\text{-AR binding}} &= \Delta\Delta G_{cisY,\beta_2\text{-AR} \rightarrow \beta_1\text{-AR}} - \Delta\Delta G_{cisX,\beta_2\text{-AR} \rightarrow \beta_1\text{-AR}} \\ &= (\Delta G_{cisY,\beta_1\text{-AR}} - \Delta G_{cisY,\beta_2\text{-AR}}) - (\Delta G_{cisX,\beta_1\text{-AR}} \\ &\quad - \Delta G_{cisX,\beta_2\text{-AR}}) \\ &= (\Delta G_{cisY,\beta_1\text{-AR}} - \Delta G_{cisX,\beta_1\text{-AR}}) - (\Delta G_{cisY,\beta_2\text{-AR}} \\ &\quad - \Delta G_{cisX,\beta_2\text{-AR}}) \\ &= \Delta\Delta G_{\text{binding},cisX \rightarrow cisY,\beta_1\text{-AR}} - \Delta\Delta G_{\text{binding},cisX \rightarrow cisY,\beta_2\text{-AR}} \end{aligned} \quad (5)$$

$$\begin{aligned} \Delta\Delta G_{\text{binding,cis(WT)} \rightarrow \text{cis(Mut)}} & \\ &= \Delta G_{\text{binding,cis(Mut)}} - \Delta G_{\text{binding,cis(WT)}} \\ &= \Delta G_{\text{cis,Mutation(holo)}} - \Delta G_{\text{Mutation(apo)}} \end{aligned} \quad (6)$$

$$\begin{aligned} \Delta\Delta G_{\text{binding,trans(WT)} \rightarrow \text{trans(Mut)}} & \\ &= \Delta G_{\text{binding,trans(Mut)}} - \Delta G_{\text{binding,trans(WT)}} \\ &= \Delta G_{\text{trans,Mutation(holo)}} - \Delta G_{\text{Mutation(apo)}} \end{aligned} \quad (7)$$

$$\begin{aligned} \Delta\Delta\Delta G_{\text{WT} \rightarrow \text{Mut,cis-vs-trans binding}} & \\ &= \Delta\Delta G_{\text{binding,trans(WT)} \rightarrow \text{trans(Mut)}} - \Delta\Delta G_{\text{binding,cis(WT)} \rightarrow \text{cis(Mut)}} \\ &= [\Delta G_{\text{binding,trans(Mut)}} - \Delta G_{\text{binding,trans(WT)}}] \\ &\quad - [\Delta G_{\text{binding,cis(Mut)}} - \Delta G_{\text{binding,cis(WT)}}] \\ &= [\Delta G_{\text{trans,Mutation(holo)}} - \Delta G_{\text{Mutation(apo)}}] \\ &\quad - [\Delta G_{\text{cis,Mutation(holo)}} - \Delta G_{\text{Mutation(apo)}}] \\ &= \Delta G_{\text{trans,Mutation(holo)}} - \Delta G_{\text{cis,Mutation(holo)}} \end{aligned} \quad (8)$$

In Approach A, the *cis* isomer of each compound X is alchemically transformed to the *trans* isomer in the TI simulation via an unphysical pathway, with one phenyl ring gradually disappearing from one side of the N=N double bond and reappearing on the other side (Figure 3).

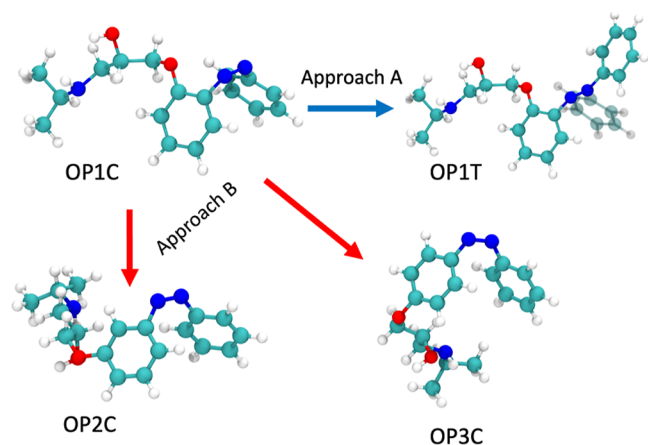


Figure 3. Two different approaches (Approach A and Approach B) for calculating the substituents' effects on the *cis-vs-trans* affinity differential of the antagonists. In Approach A, for the same compound, e.g., OP1, the *cis* isomer (OP1C) is converted to the *trans* isomer (OP1T) through the disappearance of a functional group from one side of the N=N bond and the reappearance of it on the other side. In approach B, the side-chain substituent is moved to different positions on the benzyl ring within the same isomeric form. For example, the *cis* isomer of OP1 (OP1C) is converted to the *cis* isomer of OP2 (OP2C) or OP3C.

The free energy differences between the two isomers in protein ($\Delta G_{\text{bound,cisX} \rightarrow \text{transX}}$) and the aqueous solution ($\Delta G_{\text{unbound,cisX} \rightarrow \text{transX}}$) were directly estimated by the TI simulations. Then, a thermodynamic cycle (Figure 2A) was constructed to estimate the *cis-vs-trans* affinity differential of the compound X, i.e., $\Delta\Delta G_{X,\text{cis} \rightarrow \text{trans}}$ using eq 1. In Approach B, one compound X is transformed to the other compound Y in the same isomeric form by alchemically removing and adding the differing groups between the two compounds (Figure 3). The free energy differences between the two compounds in protein ($\Delta G_{\text{cisX} \rightarrow \text{cisY,bound}}$ and $\Delta G_{\text{transX} \rightarrow \text{transY,bound}}$) and in the aqueous solution ($\Delta G_{\text{cisX} \rightarrow \text{cisY,unbound}}$ and $\Delta G_{\text{transX} \rightarrow \text{transY,unbound}}$) were directly

estimated. A thermodynamic cycle (Figure 2B) was constructed to estimate the difference in the binding affinities between the compound X and Y in the same isomeric form, i.e., $\Delta\Delta G_{\text{binding,cisX} \rightarrow \text{cisY}}$ and $\Delta\Delta G_{\text{binding,transX} \rightarrow \text{transY}}$ using eqs 2 and 3. Using the above-described relative binding affinities, the substituent's effect on the *cis-vs-trans* affinity differential, i.e., the $\Delta\Delta\Delta G_{X \rightarrow Y,\text{cis-vs-trans binding}}$ can be estimated from either approach using eq 4.

Based on the available experimental data,^{7,32} the S enantiomer exhibits a stronger “*cis-on*” effect than the R enantiomer (Figure 1) in β_2 -AR. In addition, the S enantiomer of OP2 exhibits higher binding affinity than the R enantiomer in both the *cis* and *trans* isomers. Because experimental measurements are available for both R and S only for OP2,³² and the S enantiomer consistently exhibits stronger receptor affinity, all simulations in this study were performed using the S enantiomer of the OP compounds, except for OP2, for which both R and S enantiomers were simulated. In addition, according to the experimental reports, the PLZ compounds were synthesized and evaluated in the S enantiomeric form.³¹ To further evaluate the effect of chirality, TI calculations using Approach B, MM/PBSA and MM/GBSA simulations were also carried out to estimate the relative binding free energy difference between the S and R enantiomers.

Additionally, using Approach B, the substituent's effect on the binding selectivity between β_1 -AR and β_2 -AR in the same isomeric form, e.g., $\Delta\Delta\Delta G_{X \rightarrow Y,\beta_1\text{-AR vs } \beta_2\text{-AR binding(cis or trans)}}$ was calculated. This quantity describes the effect of X→Y transformation on the relative binding affinity between the β_1 -AR and β_2 -AR. This calculation began with the TI evaluation of the free energy change associated with alchemical transformations between the two compounds in the same isomeric form in both the β_1 -AR and β_2 -AR, as well as in solution. Based on these quantities, employing a thermodynamic cycle in Figure 2B, the difference in the binding affinity between the two compounds with the β_1 -AR (e.g., $\Delta\Delta G_{\text{binding,cisX} \rightarrow \text{cisY},\beta_1\text{-AR}}$) and the β_2 -AR (e.g., $\Delta\Delta G_{\text{binding,cisX} \rightarrow \text{cisY},\beta_2\text{-AR}}$) was calculated. The $\Delta\Delta\Delta G_{X \rightarrow Y,\beta_1\text{-AR vs } \beta_2\text{-AR binding}}$ value was finally calculated according to eq 5.

Furthermore, to assess the effect of the mutation on the *cis-vs-trans* affinity of OP2, TI calculations were performed in a β_2 -AR mutant. In these simulations, the PHE289 residue in the wild-type (WT) receptor was gradually transformed into the alanine residue, generating the mutant receptor (Mut), by systematically modifying the system Hamiltonian using a λ parameter ranging from 0 to 1 (with a spacing of 0.1). From each TI calculation, the free energy change associated with the mutation was obtained for the entire system in both the OP2-unbound (apo) and OP2-bound (holo) states of β_2 -AR, yielding $\Delta G_{\text{Mutation(apo)}}$ and $\Delta G_{\text{Mutation(holo)}}$, respectively. A thermodynamic cycle (Figure 2C) was then used to determine the mutation-induced changes in OP2 binding free energy in the *cis* and *trans* isomers, expressed as $\Delta\Delta G_{\text{binding,cis(WT)} \rightarrow \text{cis(Mut)}}$ and $\Delta\Delta G_{\text{binding,trans(WT)} \rightarrow \text{trans(Mut)}}$ (eqs 6 and 7). A positive $\Delta\Delta G_{\text{binding}}$ value indicates reduced binding affinity upon mutation. Based on these relative binding affinities, the effect of the mutation on the *cis-vs-trans* affinity differential, defined as $\Delta\Delta\Delta G_{\text{WT} \rightarrow \text{Mut,cis-vs-trans binding}}$ was calculated using eq 8. A positive $\Delta\Delta\Delta G_{\text{WT} \rightarrow \text{Mut,cis-vs-trans binding}}$ value indicates that the mutation enhances the “*cis-on*” effect in β_2 -AR compared with the wild-type receptor.

In the TI calculation, the set of atoms differing between the starting and ending compounds linked by the alchemical transition (X→Y) was separated into two sets: atoms disappearing from X and those appearing in Y. The TI simulation was divided into three stages: (1) switching off the charges on the disappearing atoms to zero, (2) switching off the van der Waals and bonded interactions associated with the disappearing atom and switching on these interactions associated with the appearing atoms, while keeping all charges on both sets of atoms zero (3) switching on the charges on the appearing atoms to full charge. In each stage of each TI simulation, 11 λ windows were simulated, with a λ spacing of 0.1, totaling 33 windows

per alchemical transformation. The soft-core potential was applied to their van der Waals interactions of the disappearing and appearing atoms in stage (2).

To prepare the initial structure of the TI simulation, the system was equilibrated in a mixed Hamiltonian of X and Y, corresponding to the $\lambda = 0.5$ in stage (2), except that both disappearing and appearing atoms have full charges. The initial geometries of the systems were taken from a representative snapshot in the unbiased MD equilibrated simulation for one of the two compounds. The system was minimized using 15,000 steepest descent steps, and then reheated to 300 K over a period of 1 ns using the Langevin thermostat⁷⁷ with a friction coefficient of 1 ps^{-1} . Following this, the systems were equilibrated for 20 ns in the constant *NPT* ensemble (300 K, 1 bar) without positional restraints. The last snapshot was subsequently used as the initial structure in each λ window in each of the three stages. In each λ window, 500 ps of *NVT* equilibration and at least 6 ns of production *NPT* simulations were performed.

Furthermore, TI calculations were performed to quantify the effect of the F289A mutation on OP2's light-responsive affinity differential in β_2 -AR. In both the apo and holo states of the receptor, the PHE289 residue was alchemically transformed into alanine using a dual-topology scheme implemented in AMBER,⁸⁰ with the mutation gradually introduced through a coupling parameter (λ) ranging from 0 to 1. A total of 11 λ windows were used with an interval of 0.1. The mutation region was defined using the corresponding TI masks for the WT and mutant residues. Each λ window followed a standard three-step protocol including energy minimization, heating, and production. During minimization, positional restraints were applied to the solute while the system was relaxed. The systems were then gradually heated to 300 K temperature under constant volume using a Langevin thermostat,⁷⁷ followed by production simulations performed in the constant *NPT* ensemble at 300 K temperature and 1 atm pressure. In each λ window, 500 ps of constant *NVT* equilibration and at least 50 ns of production *NPT* simulations were performed. The error bars in the TI calculations were obtained by block-average analysis.

In the TI simulations performed, SHAKE constraints were applied to the system except for bonds connecting one common and softcore atom(s), which is the default option in the AMBER simulation package.⁸⁰ This is to ensure stable integration during the alchemical process.⁷⁹ Because these bond constraints are removed, a 1 fs time step was used.⁸¹ It is worth noting that using a 1 fs time step increases the computational cost compared with simulations that use SHAKE for the whole system and a 2 fs time step. However, this choice reduces the risk of numerical instability during the alchemical transformations.

Umbrella Sampling (US) and Well-Tempered Metadynamics (WT-MTD)

To estimate the *cis-vs-trans* affinity differential of each ligand, the potential of mean force (PMF) of its thermal isomerization in protein and aqueous solution was calculated by both US and WT-MTD simulations.²⁷ The *cis-vs-trans* affinity differential $\Delta\Delta G_{X,cis \rightarrow trans}$ was then estimated using the PMFs in the protein and solution through the thermodynamic cycle in Figure 2A. The $\Delta\Delta\Delta G_{X \rightarrow Y,cis \rightarrow trans \text{ binding}}$ was calculated using $\Delta\Delta G_{X,cis \rightarrow trans}$ (eq 4).

In the US simulations, the torsion around the N=N double bond, i.e., $\theta_{\text{C}_{\text{NNC}}}$ (Figure 1A), was the collective variable (CV) biased in the simulations and used for projecting the 1-dimensional PMFs. A total of 37 umbrella windows were used for each PMF. The centers of harmonic potentials used in the windows were positioned at different values from 0° to 180° with a 5° interval. In each window, the harmonic potential had a force constant of $200 \text{ kcal/mol/radian}^2$. The final frame of the MD production trajectory of the *cis* isomer served as the starting point for the first umbrella window. The initial structure for each window was derived from the adjacent window's structure after a 1 ns equilibration period. Afterward, at least 20 ns of production simulation was performed for each window, which was used for analysis. In total, at least 740 ns of US production run was conducted for each system, in the protein or solution. The PMF was

constructed using the WHAM algorithm.⁸² The US simulations were performed using the AMBER24 software package interfaced with PLUMED 2.9.⁸³ The error bars in the PMFs were calculated by block-average analysis.

In the WT-MTD simulations, two CVs were biased in the simulation and used in the projection of the 2D PMFs: $\text{CV1} = \theta_{\text{C}_{\text{NNC}}}$, $\text{CV2} = \frac{1}{2}(\theta_{\text{C}_{1\text{C}2\text{NN}}} + \theta_{\text{N}_{\text{NC}5\text{C}6}})$. The CV2 is the average of the two torsions around the single bonds adjacent to the N=N double bond (Figures 1B and S1). The deposition rate, width, bias factor, and initial height of the Gaussians were set to 2.0 ps^{-1} , 0.35 radians, 45, and 2.5 kJ/mol , respectively. For each system, 500 and 100 ns WT-MTD simulations were conducted for the protein–ligand complex and ligand in the aqueous solution, respectively, using a 2 fs time step. All WT-MTD simulations were performed using the AMBER24 interfaced with the PLUMED 2.9 packages.

MM/PBSA and MM/GBSA

The final 150 ns of the production step was used to evaluate the binding affinity of the ligands against β_1 -AR and β_2 -AR using MM/PBSA or MM/GBSA methods. In these calculations, dielectric constants of 80, 2, and 4 were assigned to water, the lipid membrane, and the protein, respectively.^{84,85} A solvent probe radius of 1.4 \AA was used, and the default force field parameters were applied for the atomic radii.⁸⁶ The $\Delta\Delta G_{X,cis \rightarrow trans}$ values were calculated directly using the absolute binding affinities obtained from the MM/PBSA and MM/GBSA simulations of different isomers (eq 1). The $\Delta\Delta\Delta G_{X \rightarrow Y,cis \rightarrow trans \text{ binding}}$ was calculated using $\Delta\Delta G_{X,cis \rightarrow trans}$ (eq 4). The error bars in the calculations were obtained by block-average analysis.

RESULTS AND DISCUSSION

This section is organized as follows. First, we systematically compare the accuracy of different free energy methods in predicting the substituents' effect on the difference in the binding affinity between *cis* and *trans* isomers (referred to as "*cis-vs-trans* affinity differential" below) among three OPs: OP1, OP2, and OP3 in β_2 -AR and β_1 -AR, identifying the compound-to-compound TI approach as the most accurate one. Second, we extensively benchmark the accuracy of these approaches in four additional scenarios with crucial implications in previous experimental designs: (1) comparison between PLZs and OPs in terms of the *cis-vs-trans* affinity differential in β_2 -AR and β_1 -AR; (2) enantiospecific effects on the *cis-vs-trans* affinity differential of OPs in β_2 -AR; (3) the OPs' selectivity between the β_1 -AR and β_2 -AR subtypes; (4) substituents' effect on the *cis-vs-trans* affinity differential in β_2 -AR among PLZs; (5) the effect of the mutation on light-responsive binding affinity differential of OP2. The experimental binding affinities were deduced from photostationary states (PSS) under different wavelengths of light, where either the *trans* or *cis* isomer predominates.^{7,31,32} For the OPs, the binding affinities (K_i values) were directly measured.^{7,32} For the PLZs, only functional studies were performed, and we assumed that the K_i values deduced from the IC_{50} 's of these bioactivity measurements were equal to the binding affinities (K_i values). Third, we present a detailed analysis of protein–ligand interactions based on unbiased MD simulations, which reveals the molecular origin of the light-responsive binding affinity of these ligands. Finally, we discuss several key details of our free energy simulations.

Throughout the discussion, we refer to the thermodynamic cycles in Figure 2 and eqs 1–8 in the Method section for the definition and calculation of the absolute binding free energies, relative binding free energies, and the substituents' effect on them. In particular, eq 1 was used for the relative binding

Table 1. Calculated *cis*-vs-*trans* Affinity Differential ($\Delta\Delta G_{X,cis \rightarrow trans}$) in β_2 -AR and β_1 -AR Using the Approach A of the TI Method (*cis*-to-*trans*), US, TI, WT-MTD, MM/PBSA, and MM/GBSA, Compared to the Experiment^{7a}

quantity	compounds		
	OP1	OP2	OP3
	β_2 -AR		
$\Delta\Delta G_{X,cis \rightarrow trans}$ (Exp.)	-0.8 ± 0.6	3.8 ± 0.6 (racemic mixture) 4.1 ± 0.3 (OP2(S))	0.5 ± 0.1
$\Delta\Delta G_{X,cis \rightarrow trans}$ (TI)	0 ± 1	1 ± 1	2.2 ± 0.3
$\Delta\Delta G_{X,cis \rightarrow trans}$ (US)	-5.5 ± 0.1	8.6 ± 0.5	2.7 ± 0.2
$\Delta\Delta G_{X,cis \rightarrow trans}$ (WT-MTD)	-3.0 ± 3.8	1.0 ± 2.0	0.6 ± 2.2
$\Delta\Delta G_{X,cis \rightarrow trans}$ (MM/PBSA)	0.6 ± 0.1	-3.0 ± 0.1	10.1 ± 0.1
$\Delta\Delta G_{X,cis \rightarrow trans}$ (MM/GBSA)	-4.9 ± 0.1	-3.1 ± 0.1	12.2 ± 0.1
	β_1 -AR		
$\Delta\Delta G_{X,cis \rightarrow trans}$ (Exp.)	-1.3 ± 0.1	1.9 ± 0.1	-1.7 ± 0.3
$\Delta\Delta G_{X,cis \rightarrow trans}$ (US)	-3.1 ± 1.1	9.3 ± 0.9	-4.6 ± 0.7
$\Delta\Delta G_{X,cis \rightarrow trans}$ (MM/PBSA)	-5.1 ± 0.1	11.0 ± 0.1	0.8 ± 0.1
$\Delta\Delta G_{X,cis \rightarrow trans}$ (MM/GBSA)	-4.0 ± 0.1	9.2 ± 0.1	-2.9 ± 0.1

^aApproach A of TI and WT-MTD were used to calculate *cis*-vs-*trans* affinity differential in β_2 -AR. The other methods were applied to calculate the $\Delta\Delta G_{X,cis \rightarrow trans}$ for both receptors. A positive value of $\Delta\Delta G_{X,cis \rightarrow trans}$ indicates a higher binding affinity in the *cis* isomer than in the *trans* isomer, and vice versa. All calculations reported in this table were performed in the S enantiomer. The experimental values were reported for the racemic mixture of S and R isomers, unless otherwise noted for OP2, where the enantiospecific $\Delta\Delta G_{X,cis \rightarrow trans}$'s were also measured.³² Table S1 contains the detailed information on quantities calculated by each method.

Table 2. Calculated Difference in the binding Free Energies $\Delta\Delta G_{\text{binding},X \rightarrow Y}$ (kcal/mol) between the OPs in the Same Isomeric Form (Either *cis* or *trans*) in β_2 -AR and β_1 -AR Using Approach B of the TI Method (Compound-to-Compound) Compared to the Experiment^{7,a}

quantities	chemical modifications			
	OP1C→OP2C	OP1T→OP2T	OP2C→OP3C	OP2T→OP3T
	β_2 -AR			
$\Delta\Delta G_{\text{binding},X \rightarrow Y}$ (Exp.)	-0.1 ± 0.6	4.5 ± 0.6	4.4 ± 0.4	1.1 ± 0.4
$\Delta\Delta G_{\text{binding},X \rightarrow Y}$ (TI)	-1.1 ± 0.9	3.2 ± 0.8	4.1 ± 0.3	1.6 ± 0.4
	β_1 -AR			
$\Delta\Delta G_{\text{binding},X \rightarrow Y}$ (Exp.)	0.6 ± 0.1	3.8 ± 0.2	0.0 ± 0.1	-3.5 ± 0.6
$\Delta\Delta G_{\text{binding},X \rightarrow Y}$ (TI)	1.5 ± 0.5	3.1 ± 0.8	0.0 ± 0.6	-3.3 ± 1.4

^aA negative value of $\Delta\Delta G_{\text{binding},X \rightarrow Y}$ indicates a higher binding affinity in the ending compound than in the starting compound, and vice versa. All calculations reported in this table were performed in the S enantiomer. The experimental values were reported for the racemic mixture of S and R enantiomers. Table S3 contains the detailed information on quantities calculated from the TI simulations using Approach B.

affinities between *cis* and *trans* isomers of the same compound X, i.e., the light-responsive affinity differential. eqs 2 and 3 were used for the relative binding affinities between the same isomer of compounds X and Y. Equation 4 was used for the substituents' effects on the light-responsive binding affinity differential. Equation 5 was used for substituents' effects on the subtype selectivity between the β_1 -AR and β_2 -AR. Equations 6–8 were used for mutational effects on the light-responsive affinity differential.

Method Comparison: The Light-Responsive Affinity Differential of OPs in β_2 -AR and β_1 -AR

Five free energy methods, namely the TI, US, WT-MTD, MM/GBSA, and MM/PBSA were employed to predict the substituents' effects on the light-responsive affinity differential for three antagonists, i.e., OP1, OP2, and OP3, in β_2 -AR and β_1 -AR. Each method was benchmarked against experimental isomer-specific binding affinities.^{7,31,32}

Thermodynamic Integration (TI)

The TI method has been well-regarded as one of the most accurate methods for estimating relative binding affinities between different ligands. For this reason, we first test its accuracy in quantifying how chemical modifications, i.e., changing from compound X to Y (X and Y being two of the OP1, OP2, and OP3 compounds), affect the *cis*-vs-*trans* affinity differential in β_2 -AR and β_1 -AR ($\Delta\Delta\Delta G_{X \rightarrow Y, cis \rightarrow trans \text{ binding}}$ Method).

We employed two approaches with different alchemical transformation pathways to compare their performance. In the first one (Approach A), the TI simulations alchemically converted the *cis* isomer of the photoswitch into its *trans* isomer (Figure 3). The *cis*-to-*trans* alchemical transformations were performed in both the aqueous solution and the β_2 -AR, and the *cis*-vs-*trans* affinity differential of compounds X and Y ($\Delta\Delta G_{X,cis \rightarrow trans}$ and $\Delta\Delta G_{Y,cis \rightarrow trans}$) were directly calculated through a thermodynamic cycle (Method, Figure 2A, eqs 1 and 2). The difference between the two compounds' *cis*-vs-

trans affinity differentials, i.e., $\Delta\Delta\Delta G_{X \rightarrow Y, cis-vs-trans \text{ binding}}$, can be calculated by taking the difference of these two $\Delta\Delta G$'s (Method, eq 4). Thus, this quantity is key to measuring the substituent's effect on the light-responsive affinity differential. A positive $\Delta\Delta\Delta G_{X \rightarrow Y, cis-vs-trans \text{ binding}}$ indicates a higher "cis-on" effect in the ending compound (Y) than in the starting compound (X), and *vice versa*. The calculated $\Delta\Delta G_{X, cis \rightarrow trans}$ and $\Delta\Delta\Delta G_{X \rightarrow Y, cis-vs-trans \text{ binding}}$ values using Approach A, together with the experimental ones, are reported in Tables 1 and 3.

Table 3. Calculated Substituents' Effects on the *cis-vs-trans* Affinity Differential ($\Delta\Delta\Delta G_{X \rightarrow Y, cis-vs-trans \text{ binding}}$, in kcal/mol) in the β_2 -AR and β_1 -AR Using the TI (Approaches A & B), US, WT-MTD, MM/PBSA, and MM/GBSA Methods Compared to the Experiment^{7,a}

approach	$\Delta\Delta\Delta G_{X \rightarrow Y, cis-vs-trans \text{ binding}}$		
	OP1 \rightarrow OP2	OP2 \rightarrow OP3	OP1 \rightarrow OP3
β_2 -AR			
experiment	4.6 \pm 0.8	-3.3 \pm 0.6	1.3 \pm 0.6
TI (Approach A)	1 \pm 1	1 \pm 1	2 \pm 1
TI (Approach B)	4 \pm 1	-2.5 \pm 0.5	2 \pm 1
US	14.1 \pm 0.5	-5.9 \pm 0.5	8.2 \pm 0.2
WT-MTD	4.0	-0.4	3.6
MM/PBSA	-3.6 \pm 0.1	13.1 \pm 0.1	9.5 \pm 0.1
MM/GBSA	1.8 \pm 0.1	15.3 \pm 0.1	17.1 \pm 0.1
β_1 -AR			
experiment	3.2 \pm 0.2	-3.5 \pm 0.3	-0.3 \pm 0.4
TI (Approach B)	1.6 \pm 0.9	-3.3 \pm 1.5	-1.7 \pm 1.7
US	12.4 \pm 1.4	-13.9 \pm 1.1	-1.5 \pm 1.3
MM/PBSA	16.1 \pm 0.1	-10.2 \pm 0.1	5.9 \pm 0.1
MM/GBSA	13.2 \pm 0.1	-12.1 \pm 0.1	1.1 \pm 0.1

^aA Positive Value of $\Delta\Delta\Delta G_{X \rightarrow Y, cis-vs-trans \text{ binding}}$ Indicates a Higher "cis-on" Effect in the Ending Compound Than in the Starting Compound, and *Vice Versa*.

In the second approach (Approach B), one compound was converted to another in the same isomeric form (Figure 3) in both the aqueous solution and the β_2 -AR and β_1 -AR, in both the *cis* and *trans* isomers. In the alchemical transformation, the entire 3-(isopropylamino)-2-hydroxypropoxy (IHP) side chain gradually disappears from the benzyl carbon atom to which it is linked and reappears on another one. For example, when transforming the *cis* OP1 (OP1C) to *cis* OP2 (OP2C), the position of the side chain disappears from the ortho position on the phenyl ring and is changed to the meta position (Figure 3). Performing the TI simulations for this transformation in the protein and aqueous solution and employing another thermodynamic cycle (Figure 2B, eq 2), the relative binding free energy between OP1C and OP2C can be calculated, i.e., $\Delta\Delta G_{\text{binding}, OP1C \rightarrow OP2C}$. Similar calculations were performed on the *trans* isomers of OP1 and OP2 (OP1T and OP2T) using eq 3, generating $\Delta\Delta G_{\text{binding}, OP1T \rightarrow OP2T}$. Finally, the $\Delta\Delta\Delta G_{OP1 \rightarrow OP2, cis-vs-trans \text{ binding}}$ values were calculated by taking the difference of these two $\Delta\Delta G$'s (Method, eq 4). The calculated $\Delta\Delta G_{\text{binding}, X \rightarrow Y}$ and $\Delta\Delta\Delta G_{X \rightarrow Y, cis-vs-trans \text{ binding}}$ values using Approach B, together with the experimental ones, are reported in Tables 2 & 3.

Employing Approach A, the calculated values of *cis-vs-trans* affinity differential for the three OPs are in qualitative agreement with the experimental values (Table 1), predicting the active isomer of the photoswitch for each compound. For the OP2, the positive $\Delta\Delta G$ values indicate that the OP2 has "cis-on" activity, i.e., the thermodynamically less stable *cis* isomer, which dominates the photostationary state under 360 nm light, has higher antagonist activity against the β_2 -AR than the more stable *trans* isomer. The "cis-on" effect is also observed for OP3 (Table 1). However, Approach A cannot always accurately predict the substituents' effects on the *cis-vs-trans* affinity differential ($\Delta\Delta\Delta G_{X \rightarrow Y, cis-vs-trans \text{ binding}}$) between two different compounds (Table 3). For example, experimental values of $\Delta\Delta\Delta G_{X \rightarrow Y, cis-vs-trans \text{ binding}}$ show that OP2 has a greater "cis-on" effect than OP3 (Table 3). In contrast, the TI method predicts that OP3 has a greater "cis-on" effect than OP2 by 1 ± 1 . Therefore, Approach A is accurate for evaluating the *cis-vs-trans* affinity differential within a single compound, but sometimes fail to predict how chemical modifications can change this quantity.

Using Approach B, the calculated relative binding affinities between these three antagonists in the same isomer form ($\Delta\Delta G_{\text{binding}, X \rightarrow Y}$) in complex with β_1 -AR and β_2 -AR were calculated (Table 2, $\Delta\Delta G_{\text{binding}, X \rightarrow Y}$), based on which the substituents' effect on the *cis-vs-trans* affinity differential ($\Delta\Delta\Delta G_{X \rightarrow Y, cis-vs-trans \text{ binding}}$) was calculated (Table 3).

According to Table 2, the calculated $\Delta\Delta G_{\text{binding}, OP1C \rightarrow OP2C}$ of -1.1 ± 0.9 kcal/mol indicates that the *cis* OP1 to *cis* OP2 transformation increases the ligand's binding affinity in β_2 -AR. In contrast, the corresponding value of 1.5 ± 0.5 kcal/mol for β_1 -AR indicates a reduction in binding affinity for the same transformation. These trends are consistent with the experimental results, which report -0.1 ± 0.6 kcal/mol for β_2 -AR, within the error bars, and 0.6 ± 0.1 kcal/mol for β_1 -AR. The calculated $\Delta\Delta G_{\text{binding}, OP1T \rightarrow OP2T}$ of 3.2 ± 0.8 kcal/mol indicates that the *trans* OP1 to *trans* OP2 transformation decreases the ligand's binding affinity in β_2 -AR, in agreement with the experimental value of 4.5 ± 0.6 kcal/mol. The same trend is observed for β_1 -AR, where the calculated $\Delta\Delta G_{\text{binding}, OP1T \rightarrow OP2T}$ is 3.1 ± 0.8 kcal/mol, consistent with the corresponding experimental values of 3.8 ± 0.2 kcal/mol.

The calculated $\Delta\Delta G_{\text{binding}, OP2C \rightarrow OP3C}$ and $\Delta\Delta G_{\text{binding}, OP2T \rightarrow OP3T}$ for β_2 -AR are also consistent with experimental observations, indicating that transforming OP2 to OP3 in either the *cis* or *trans* isomer forms decreases the binding affinity. For β_1 -AR, a different behavior is observed. The calculated $\Delta\Delta G_{\text{binding}, OP2C \rightarrow OP3C}$ is 0.0 ± 0.6 kcal/mol, indicating essentially no change in binding affinity for the *cis* transformation, in agreement with the experimental value of 0.0 ± 0.1 kcal/mol. In contrast, converting *trans* OP2 to *trans* OP3 increases the binding affinity in β_1 -AR, as reflected by the calculated $\Delta\Delta G_{\text{binding}, OP2T \rightarrow OP3T}$ value of -3.3 ± 1.4 kcal/mol, which differs from the trend observed in β_2 -AR.

The $\Delta\Delta\Delta G_{X \rightarrow Y, cis-vs-trans \text{ binding}}$ values for the OP1 \rightarrow OP2, OP2 \rightarrow OP3, and OP1 \rightarrow OP3 transformations were also accurately predicted by Approach B (Table 3) for both β_1 -AR and β_2 -AR. For the OP1 \rightarrow OP2 transformation in β_2 -AR, both experimental (4.6 ± 0.8 kcal/mol) and theoretical (4 ± 1 kcal/

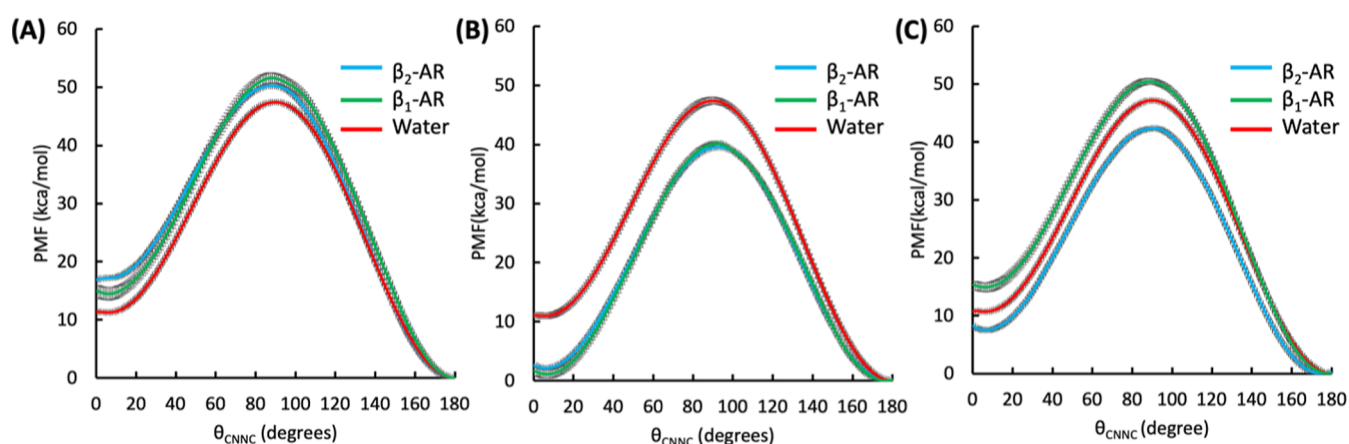


Figure 4. Potential of mean forces (PMFs) for the ground-state *cis*-to-*trans* isomerization of the photoswitchable ligands in complex with the β_2 -AR (blue), β_1 -AR (green), and in an aqueous environment (red), calculated by the US method. The results are shown for (A) OP1, (B) OP2, and (C) OP3. The *trans* isomer of each compound corresponds to the minima near $\theta_{\text{CNCC}} = 180^\circ$. The *cis* isomer of each compound corresponds to the minima near $\theta_{\text{CNCC}} = 0^\circ$.

mol) results show an increase in the “*cis*-on” effect. A similar trend is also observed in β_1 -AR, where the calculated value of 1.6 ± 0.9 kcal/mol suggests an increase in the *cis* preference for this transformation. For the OP2→OP3 transformation in β_2 -AR, both experimental (-3.3 ± 0.6 kcal/mol) and theoretical (-2.5 ± 0.5) values indicate a decrease in the “*cis*-on” effect (Table 3). Note that Approach A failed to capture this behavior correctly, as it predicted the wrong sign for $\Delta\Delta\Delta G_{\text{OP2} \rightarrow \text{OP3}, \text{cis-vs-trans binding}}$ (Table 3). A similar behavior is observed for β_1 -AR. For the OP2 → OP3 transformation, the TI calculated $\Delta\Delta\Delta G_{\text{OP2} \rightarrow \text{OP3}, \text{cis-vs-trans binding}}$ value of -3.3 ± 1.5 kcal/mol is in very good agreement with the experimental result of -3.5 ± 0.3 kcal/mol (Table 3). The negative sign indicates a reduction in the “*cis*-on” effect upon transforming OP2 to OP3 and confirms that the TI calculations capture how this structural modification shifts the *cis*-vs-*trans* binding preference in both receptors.

Thus, Approach B can reliably capture all subtle substituents’ effects on the light-responsive affinity differential among the three OPs, highlighting its predictive power in the design and optimization of light-responsive bioactivity of photoswitchable drugs targeting GPCRs. Notably, in our recent parallel study of photoswitchable inhibitors of tubulin, this method has also achieved good agreement with the experiments.¹⁸

Umbrella Sampling (US)

Next, we benchmarked the US method (Figure 4), a widely used enhanced-sampling technique for free energy calculation. The torsion around the N=N double bond, i.e., θ_{CNCC} (Figure 1B), was used as the collective variable (CV) biased in simulations and the projection of 1-dimensional PMFs. The PMFs describe the free energy profile of ground-state *cis*-to-*trans* isomerization of OP1, OP2, and OP3 in both the β_2 -AR, β_1 -AR, and aqueous solution. The free energy difference between the *cis* and *trans* isomer forms in either the proteins or the solution, i.e., $\Delta G_{\text{bound}, \text{cis} \rightarrow \text{trans}}$ and $\Delta G_{\text{unbound}, \text{cis} \rightarrow \text{trans}}$ was evaluated based on the 1D PMF’s two minima (Figure 4), where θ_{CNCC} is $\sim 0^\circ$ and $\sim 180^\circ$, respectively. Similar to the Approach A of the TI method, the thermodynamic cycle in Figure 2A was adopted to calculate the $\Delta\Delta G_{X, \text{cis} \rightarrow \text{trans}}$ and $\Delta\Delta\Delta G_{X \rightarrow Y, \text{cis-vs-trans binding}}$ values using eq 4. Here, the key

difference between the US and Approach A of TI method is that the US samples a realistic ground-state thermal relaxation pathway connecting the two isomers with a physics-based free energy barrier, whereas the TI simulations involve unphysical, alchemical transitions where different functional groups gradually disappear and appear in different positions. Such a difference is not only theoretical but also can have practical implications in terms of sampling and convergence, as discussed below.

For all three compounds in complex with β_2 -AR, the US method correctly predicts the more bioactive isomer, i.e., the sign of $\Delta\Delta G_{X, \text{cis} \rightarrow \text{trans}}$, although the magnitudes are largely overestimated (Table 1). Importantly, throughout the simulations in all umbrella windows, the ligand remains bound inside the binding pocket, in contrast to the unstable binding behavior observed in the WT-MTD simulations (discussed below). The $\Delta\Delta\Delta G_{X \rightarrow Y, \text{cis-vs-trans binding}}$ values of β_2 -AR predicted by the US simulations have the correct signs for all three transformations, qualitatively capturing the substituents’ effects on the *cis*-vs-*trans* affinity differential among the three OPs.

Furthermore, for the OP compounds in complex with β_1 -AR, the US simulations reproduce the experimental preference between the *cis* and *trans* isomers, correctly predicting the signs of $\Delta\Delta G_{X, \text{cis} \rightarrow \text{trans}}$ for all three ligands (Table 1). Specifically, the simulations indicate a “*tran*-on” effect for OP1 and OP3 and a “*cis*-on” effect for OP2, consistent with the experimental observations. However, similar to the β_2 -AR results, the absolute magnitudes of the light-responsive affinity differentials are overestimated, most notably for OP2, where the US calculations predict a substantially greater “*cis*-on” effect. A key result is that OP3 exhibit different light-responsive behavior in the two subtypes, exhibiting “*trans*-on” effect in β_1 -AR and “*cis*-on” effect in β_2 -AR. The US simulations clearly reproduce the switch in the active isomer between the two receptor subtypes. In addition, the calculated $\Delta\Delta\Delta G_{X \rightarrow Y, \text{cis-vs-trans binding}}$ values for the transformations among OPs in complex with β_1 -AR correctly capture the qualitative trends observed experimentally (Table 3). These results suggest that the US approach is able to describe how substituent changes modulate the *cis*-vs-*trans* affinity differential across the OP series in β_1 -AR and β_2 -AR. Although the method overestimates the magnitudes of

these modulations, particularly for the OP1 \rightarrow OP2 and OP2 \rightarrow OP3 transformations in the β_2 -AR and β_1 -AR, respectively (Table 3), it is a reliable method for qualitatively predicting substituents' effects on *cis*-vs-*trans* affinity differential, second to Approach B of TI.

Well-Tempered Metadynamics (WT-MTD)

The WT-MTD method was also benchmarked to calculate the same ground-state *cis*-to-*trans* isomerization described above. Following previous simulation studies,¹⁷ two-dimensional PMFs were calculated using two CVs: CV1 = θ_{CNNC} , and CV2 = $\frac{1}{2}(\theta_{\text{C1C2NN}} + \theta_{\text{NNC5C6}})$, i.e., the average of the two single-bond torsions adjacent to the θ_{CNNC} (Figures 1B and S1). These two CVs were biased in the WT-MTD simulations and used for the projection of the 2D PMFs (Figure S4). The 2D PMFs were integrated over the CV2 to generate the 1D PMFs projected to CV1 (Figure S5). The calculations of $\Delta\Delta G_{X,cis \rightarrow trans}$ and $\Delta\Delta\Delta G_{X \rightarrow Y,cis\text{-vs-}trans \text{ binding}}$ follow the same approach as the US method.

The results of WT-MTD are summarized in Tables 1 and S1, Figures S4 and S5. For OP1, the $\Delta\Delta G_{\text{OP1},cis \rightarrow trans}$ value is -3.0 kcal/mol, indicating "trans-on" bioactivity, in qualitative agreement with the experimental value of -0.8 kcal/mol, while overestimating the magnitude. The calculated $\Delta\Delta G_{\text{OP2},cis \rightarrow trans}$ and $\Delta\Delta G_{\text{OP3},cis \rightarrow trans}$ are positive, indicating "cis-on" effect in its bioactivity, which are also qualitatively consistent with the experimental values (Table 1). Furthermore, the $\Delta\Delta\Delta G_{X \rightarrow Y,cis\text{-vs-}trans \text{ binding}}$ values obtained from WT-MTD simulations are 4.0, 3.6, and -0.4 kcal/mol for OP1 \rightarrow OP2, OP1 \rightarrow OP3, and OP2 \rightarrow OP3, respectively (Table 3). These results indicate that metadynamics captures the qualitative trends in the substituents' effects on light-responsive affinity differential, but it suffers from quantitative inaccuracy.

Despite the qualitative agreement with the experiments, serious limitations of WT-MTD were observed when monitoring the trajectories. One critical problem was that in many simulations, the ligands quickly dissociated from the protein after a few hundred nanoseconds, defeating the purpose of running these simulations for the ligand-bound system. It repeatedly occurred with different parameters of the Gaussian potential, deposition rates, and tempering, including those used by previous studies for similar photoswitchable ligands in tubulin.¹⁷ This made it difficult to converge the PMFs in the protein. Since WT-MTD adds time-dependent external biasing forces to constantly drive the structural transitions of the ligand (in our case, back-and-forth conversions between *cis* and *trans* isomers), it can sometimes push the system out of equilibrium and gradually cause the ligand to dissociate from the binding pocket. If it occurs, due to the ruggedness of the free energy surface, it could take a long time for the system to revisit the conformation where the ligand is bound in the protein. This time scale can be much longer than the time intervals of Gaussian potential deposition, making it difficult to converge the PMF. For example, the free energy difference between *cis* and *trans* isomers converged quickly after only ~ 50 ns (Figure S6 A). However, for the protein–ligand complex, even after 500 ns of simulation, this quantity still exhibits large fluctuations and fails to converge within this simulation time. Therefore, the instability of the ligand in the binding site makes the calculated PMFs unreliable, since the WT-MTD trajectories cannot faithfully

represent the bound state of the ligand throughout the entire simulation.

MM/PBSA and MM/GBSA

In addition to the light-responsive affinity differential that can be calculated using US, MTD, and TI methods, we examined the ability of MM/PBSA and MM/GBSA approaches to reproduce the absolute binding affinities of the photo-switchable ligands. Based on the results summarized in Tables S1 and S2, both methods predict strong binding of all OP and PLZ compounds for both *cis* and *trans* forms. However, the calculated $\Delta G_{\text{binding}}$ values are consistently much more negative than the experimental measurements. For example, while experimental affinities fall in the range of approximately -7 to -13 kcal/mol, the MM/GBSA results typically predict values between about -25 and -45 kcal/mol. This systematic shift indicates a clear overestimation of absolute binding affinity. These discrepancies highlight the limitations of MM/PBSA and MM/GBSA for predicting absolute binding affinities in GPCR systems. Both methods rely on simplified implicit solvent models and limited treatment of entropy, and they do not fully capture the complex environment of membrane proteins, protein conformational flexibility, and ligand–membrane interactions. Therefore, although MM/PBSA and MM/GBSA calculations provide a general indication that the ligands bind favorably to both receptors, they are not suitable for quantitative estimation of absolute binding affinities in this class of systems.

Furthermore, neither method can consistently and correctly predict the signs of the *cis*-vs-*trans* affinity differential for all three compounds (Table 1). In other words, they failed to even predict whether a ligand is "cis-on" or "trans-on". For instance, the MM/GBSA approach predicts that *trans* OP2 has a higher binding affinity than *cis* OP2 (in complex with β_2 -AR), i.e., "trans-on" bioactivity for OP2, opposite to the experimental observations that OP2 exhibits the largest "cis-on" effects of all three compounds. Compared to MM/GBSA, the MM/PBSA approach's performance is inferior, predicting a "cis-on" OP1 and a "trans-on" OP2 (in complex with β_2 -AR), both of which contradict the experiments. Furthermore, even when the signs of the *cis*-vs-*trans* affinity differential was predicted correctly, both methods largely overestimate their magnitudes (Table 1). For β_1 -AR, MM/GBSA and MM/PBSA calculations predict much larger $\Delta\Delta G_{X,cis \rightarrow trans}$ values for OP1 and OP2 (Table 1). For OP1 \rightarrow OP2 transformation in β_2 -AR, MM/GBSA correctly predicted a positive $\Delta\Delta\Delta G_{\text{OP1} \rightarrow \text{OP2},cis\text{-vs-}trans \text{ binding}}$ for both receptors, consistent with experiment, while MM/PBSA predicted the wrong sign (Table 3). For OP2 \rightarrow OP3 transformations in complex with β_2 -AR, neither method correctly predicts the negative sign of $\Delta\Delta\Delta G_{\text{OP1} \rightarrow \text{OP2},cis\text{-vs-}trans \text{ binding}}$ (Table 3).

Overall, neither method can consistently predict the absolute binding affinities, the experimental *cis*-vs-*trans* affinity differential, and the substituents' effects on the differential, and they often produce qualitatively wrong answers. Compared to TI calculations, the inferior performance of MM/PBSA and MM/GBSA suggests that additional factors, such as explicit solvent effects or entropic contributions, may need to be incorporated for improved accuracy. Indeed, incorporating these effects improved agreement with the experiments, as discussed above for the US method.

Table 4. Calculated and Experimental Relative binding Free Energies $\Delta\Delta G_{\text{binding},X\rightarrow Y}$ (kcal/mol) and Substituents' Effects on the *cis*-vs-*trans* Affinity Differential ($\Delta\Delta\Delta G_{X\rightarrow Y, \text{cis-vs-trans binding}}$) in the β_2 -AR for the OP2 \rightarrow PLZ2 and OP2(S) \rightarrow OP2(R) Transformations^a

quantity	chemical modifications			
	OP2 \rightarrow PLZ2		OP2(S) \rightarrow OP2(R)	
	OP2C \rightarrow PLZ2C	OP2T \rightarrow PLZ2T	OP2C(S) \rightarrow OP2C(R)	OP2T(S) \rightarrow OP2T(R)
$\Delta\Delta G_{\text{binding},X\rightarrow Y}$ (TI)	2.6 \pm 0.1	-0.5 \pm 0.5	1.7 \pm 0.2	1.1 \pm 0.5
$\Delta\Delta G_{\text{binding},X\rightarrow Y}$ (MM/GBSA)	-5.9 \pm 0.1	-1.7 \pm 0.1	8.5 \pm 0.1	9.2 \pm 0.1
$\Delta\Delta G_{\text{binding},X\rightarrow Y}$ (MM/PBSA)	-2.1 \pm 0.1	0.9 \pm 0.1	3.7 \pm 0.1	6.4 \pm 0.1
$\Delta\Delta G_{\text{binding},X\rightarrow Y}$ (Exp.)	2.5 \pm 0.4	-0.6 \pm 0.4	2.0 \pm 0.6	0.6 \pm 0.1
$\Delta\Delta\Delta G_{X\rightarrow Y, \text{cis-vs-trans binding}}$ (Exp.)	-3.1 \pm 0.5		-1.4 \pm 0.6	
$\Delta\Delta\Delta G_{X\rightarrow Y, \text{cis-vs-trans binding}}$ (TI)	-3.1 \pm 0.6		-0.6 \pm 0.5	
$\Delta\Delta\Delta G_{X\rightarrow Y, \text{cis-vs-trans binding}}$ (MM/GBSA)	4.2 \pm 0.1		0.7 \pm 0.1	
$\Delta\Delta\Delta G_{X\rightarrow Y, \text{cis-vs-trans binding}}$ (MM/PBSA)	3.0 \pm 0.1		2.7 \pm 0.1	

^aA negative value of $\Delta\Delta G_{\text{binding},X\rightarrow Y}$ indicates a higher binding affinity in the ending compound than in the starting compound, and *vice versa*. A positive value of $\Delta\Delta\Delta G_{X\rightarrow Y, \text{cis-vs-trans binding}}$ indicates a higher “*cis*-on” effect in the ending compound than in the starting compound, and *vice versa*. All calculations were performed in the S enantiomer, except for the OP2C(R) and OP2T(R).

Additional Benchmarking for Other Compounds and Receptor Subtypes

Below, we further benchmark the accuracy of the free energy methods in five additional scenarios, all of which are crucial for understanding the design principles of photoswitchable antagonists of β -ARs. Given the stability and convergence issues, WT-MTD was not further tested in these additional benchmarks.

Influence of *p*-Acetamido Modification on the Light-Responsive Affinity Differential

Photoazolols (PLZs) are another class of photoswitchable ligands derived from propranolol that display significant antagonist activity against β_2 -AR (Figure 1B).³¹ Their chemical structures closely resemble those of the OPs, except that PLZs contain an additional *p*-acetamido substituent on the azobenzene moiety (Figure 1B). Notably, although both OP2 and PLZ2 exhibit “*cis*-on” bioactivity, OP2 has a far greater light-responsive affinity differential than PLZ2.⁷ Specifically, the *cis* isomer of OP2 binds 587-fold more strongly than its *trans* isomer, whereas the *cis* PLZ2 binds only 3.6-fold more strongly than its *trans* isomer.^{7,31} Therefore, accurately predicting the change in the “*cis*-on” effect upon the OP2 \rightarrow PLZ2 transformation presents a critical benchmark, since it is directly related to maximizing the light-responsiveness of the bioactivity.

The $\Delta\Delta\Delta G_{\text{OP2}\rightarrow\text{PLZ2}, \text{cis-vs-trans binding}}$ value calculated by Approach B of the TI method (Table 4) is -3.1 ± 0.5 kcal/mol, in good agreement with the experimental value of -3.1 ± 0.6 kcal/mol. This result indicates that the OP2 exhibits a larger “*cis*-on” effect than the PLZ2. Furthermore, the TI calculation revealed distinct effects of the acetamido group on the relative binding affinity between the two compounds in the same isomeric form. For the *cis* isomers, the OP2C \rightarrow PLZ2C transformation resulted in a decrease in binding affinity, whereas for OP2T \rightarrow PLZ2T, the transformation slightly increases the binding affinity. Thus, the introduction of the *p*-acetamido group weakens the *cis* isomer's binding affinity while strengthening that of the *trans* isomer, thereby reducing the light-responsive affinity differential. The TI method can

capture the impact of a relatively minor chemical substitution on ligand–receptor interactions and the light-responsive affinity differential. In contrast, neither MM/PBSA nor MM/GBSA can correctly capture this trend qualitatively (Table 4).

Enantioselective Light-Responsive Affinity Differential in β_2 -AR

Experimental data³² showed that the S-enantiomer has a larger “*cis*-on” effect than the R-enantiomer in β_2 -AR (Figure 1). Moreover, the S-enantiomer of OP2 exhibits a greater affinity than the R-enantiomer for both the *cis* and *trans* isomers. This was an important discovery,³² as it demonstrated that both the absolute binding affinity and the light-responsiveness of binding affinity can be controlled by chirality, highlighting a crucial new design principle for photoswitchable inhibitors of GPCRs. Thus, the Approach B of TI and US methods were tested to capture these subtle effects. The calculated free energy results were reported in Tables 4 and S5. The calculated $\Delta\Delta G_{\text{binding},S\rightarrow R}$ values demonstrate that the S-enantiomer binding is more favorable to the receptor compared to the R-enantiomer, consistent with the experimental results. Furthermore, the $\Delta\Delta\Delta G_{X\rightarrow Y, \text{cis-vs-trans binding}}$ value calculated by TI is also consistent with experiment, showing a decreased “*cis*-on” effect upon converting the S to the R enantiomer. The good agreement between the simulation and experiment demonstrates the predictive power of the TI method for fine-tuning the light-responsive bioactivity via stereochemistry. The US method overestimated the magnitude of $\Delta\Delta\Delta G_{X\rightarrow Y, \text{cis-vs-trans binding}}$, but correctly predicted its sign (Table S5).

Subtype Selectivity between β_1 -AR and β_2 -AR

Due to the similarity of the two subtypes β_1 -AR and β_2 -AR, both OP2 and OP3 can bind to both receptors. Experimentally, the OP2 \rightarrow OP3 transformation shifts the ligand's binding selectivity between the two receptors toward the β_1 -AR⁷ in both isomeric forms. In other words, in both isomeric forms, OP2 favors binding with β_2 -AR over β_1 -AR, while the binding preference between the two receptors is reversed for OP3. Thus, the correct prediction of the reversal in subtype

Table 5. Difference between OP2 and OP3 in Their β_1 -AR vs β_2 -AR Selectivity ($\Delta\Delta\Delta G_{\text{OP2} \rightarrow \text{OP3}, \beta_1\text{-AR vs } \beta_2\text{-AR binding}}$) for both the *cis* and *trans* Isomers^a

quantities	TI	MM/GBSA	MM/PBSA	Exp.
$\Delta\Delta\Delta G_{\text{OP2} \rightarrow \text{OP3}, \beta_1\text{-AR vs } \beta_2\text{-AR binding}(\textit{cis})}$	-4.1 ± 0.7	17.8 ± 0.1	11.2 ± 0.1	-4.4 ± 0.4
$\Delta\Delta\Delta G_{\text{OP2} \rightarrow \text{OP3}, \beta_1\text{-AR vs } \beta_2\text{-AR binding}(\textit{trans})}$	-4.9 ± 1.5	-9.7 ± 0.1	-12.1 ± 0.1	-4.6 ± 0.5
$\Delta\Delta\Delta G_{\text{PLZ1} \rightarrow \text{PLZ2}, \textit{cis-vs-trans binding}(\beta_2\text{-AR})}$	2.5 ± 1.0	12.7 ± 0.1	4.6 ± 0.1	2.5 ± 0.3

^aA negative value indicates that the chemical transformation shifts the binding selectivity towards β_1 -AR. A positive value of this quantity indicates that the chemical transformation shifts the binding selectivity towards β_2 -AR, and *vice versa*. The substituents' effects on the *cis-vs-trans* affinity differential ($\Delta\Delta\Delta G_{X \rightarrow Y, \textit{cis-vs-trans binding}}$) for the PLZ1 \rightarrow PLZ2 transition in the β_2 -AR is also reported. A positive value of $\Delta\Delta\Delta G_{X \rightarrow Y, \textit{cis-vs-trans binding}}$ indicates a higher "cis-on" effect in the ending compound than in the starting compound, and *vice versa*.

selectivity upon OP2 \rightarrow OP3 transformation is crucial for designing photoswitches that minimize off-target toxicity by precisely targeting a particular receptor subtype on the cell membrane.

To this end, we define the quantity $\Delta\Delta\Delta G_{\text{OP2} \rightarrow \text{OP3}, \beta_1\text{-AR vs } \beta_2\text{-AR binding}(\textit{cis or trans})}$, which captures the effect of the chemical modification (OP2 \rightarrow OP3) on the binding selectivity between the two subtypes (Method, eq 5). To calculate this quantity, first, we calculated the relative binding affinity between the OP2 and OP3 in β_1 -AR and β_2 -AR in the same isomeric form. Then, the difference between the two relative binding affinities in β_1 -AR and β_2 -AR is calculated, which equals the difference between OP2 and OP3 in their β_1 -AR vs β_2 -AR selectivities, i.e., the $\Delta\Delta\Delta G_{\text{OP2} \rightarrow \text{OP3}, \beta_1\text{-AR vs } \beta_2\text{-AR binding}(\textit{cis or trans})}$ (eq 5). This quantity is dependent on the isomeric form and has a negative value if the chemical transformation shifts the binding selectivity toward β_1 -AR. The results are summarized in Table 5. For comparison, the values calculated by the MM/PBSA and MM/GBSA methods using eq 5 are also reported in Table 5.

The TI simulation results are quantitatively consistent with the experiment, showing that the OP2 \rightarrow OP3 transformation shifts the binding selectivity toward the β_1 -AR for both the *cis* and *trans* isomers. In contrast, the MM/PBSA and MM/GBSA methods consistently fail to predict the sign of this shift and largely overestimate its magnitude. The TI method accurately captures both the direction and magnitude of the shift, confirming its predictive power for the rational design of light-regulated drugs with high subtype-selectivity.

Light-Responsive Affinity Differential of PLZs in β_2 -AR

As described above, PLZs are also photoswitchable derivatives of propranolol, with an additional *p*-acetamido group in the azobenzene moiety compared to the OPs (Figure 1B). For each pair of PLZ and OP with the same index, e.g., the PLZ1 and OP1, the IHP side chain is located at the same position (ortho, meta, or para) on the azobenzene moiety (Figure 1B). The PLZs' design predated the OPs, serving as an independent set of benchmark data in addition to the OPs. Here, we benchmark Approach B of the TI, the MM/GBSA and MM/PBSA methods to quantify the change in *cis-vs-trans* affinity differential in β_2 -AR upon the PLZ1 \rightarrow PLZ2 transformation. The $\Delta\Delta G_{\text{binding, PLZ1} \rightarrow \text{PLZ2}}$ and $\Delta\Delta\Delta G_{\text{PLZ1} \rightarrow \text{PLZ2}, \textit{cis-vs-trans}}$ values are summarized in Tables 5 and Table S3.

For both isomers, the TI method predicts that the PLZ1 \rightarrow PLZ2 transformation has positive $\Delta\Delta G_{\text{binding}, X \rightarrow Y}$ values, indicating that PLZ1 has a stronger binding affinity than PLZ2, consistent with the experiment. In contrast, for OP1 \rightarrow OP2, the experiment and simulation yield slightly negative

$\Delta\Delta G_{\text{binding}, X \rightarrow Y}$ values (Table 2), indicating a slightly higher binding affinity of OP2 than OP1. This trend is opposite to the PLZ1 vs PLZ2 comparison. The TI method is thus capable of reproducing this subtle difference between these two pairs of ligands. Although the MM/PBSA and MM/GBSA qualitatively predict this trend, they both overestimate its magnitude.

Furthermore, the $\Delta\Delta\Delta G_{\text{PLZ1} \rightarrow \text{PLZ2}, \textit{cis-vs-trans binding}}$ value (Table 5, 2.5 ± 1.0 kcal/mol) is in quantitative agreement with experimental data, with a smaller magnitude than $\Delta\Delta\Delta G_{\text{OP1} \rightarrow \text{OP2}, \textit{cis-vs-trans binding}}$. Thus, adding the *p*-acetamido group to the azobenzene moiety diminishes the increase in the "cis-on" effect upon relocation of the IHP side chain. In other words, the *p*-acetamido group couples with the location of the IHP side chain to collectively influence the magnitudes of *cis-vs-trans* affinity differential. This collective effect may arise from the additional polar and hydrogen-bond interactions between the *p*-acetamido group and the receptor binding pocket. These additional protein–ligand interactions perturb the original *cis-vs-trans* affinity differential of the OPs lacking the *p*-acetamido groups. Notably, the TI method accurately predicts such a nuanced collective effect of the two substituents.

Mutational Effects on the Light-Responsive Affinity Differential

Additional TI benchmark calculations were performed to evaluate the effect of the mutation on the light-responsive affinity differential of OP2 in β_2 -AR. The change of binding affinity upon mutation was calculated using the thermodynamic cycle in Figure 2C and eqs 6 and 7. The mutational effects on the *cis-vs-trans* affinity differential, $\Delta\Delta\Delta G_{\text{WT} \rightarrow \text{Mut}, \textit{cis-vs-trans binding}}$, was calculated using eq 8. Experimental studies³² have identified PHE289 as one of the most influential residues controlling light-responsive ligand binding in β_2 -AR. Our calculated relative binding free energies between the wild-type and mutant systems closely match the experimental observations. In both experiment and simulation, the F289A mutation weakens ligand binding for both isomers, with a greater effect for the *cis* isomer. The computed relative binding affinity change upon mutation for the *cis* isomer ($\Delta\Delta G_{\text{binding}, \textit{cis}(\text{WT}) \rightarrow \textit{cis}(\text{Mut})}$) is 2.9 ± 0.1 kcal/mol and 1.1 ± 0.3 kcal/mol for the *trans* isomer ($\Delta\Delta G_{\text{binding}, \textit{trans}(\text{WT}) \rightarrow \textit{trans}(\text{Mut})}$), in good agreement with the experimental values of 3.2 ± 0.6 and 1.3 ± 0.4 kcal/mol, respectively (Table S4). Additionally, the simulation predicts a negative $\Delta\Delta\Delta G_{\text{WT} \rightarrow \text{Mut}, \textit{cis-vs-trans binding}}$ (-1.8 ± 0.3 kcal/mol), indicating a smaller "cis-on" effect in the mutant than the wild-type, in agreement with the experiment (-1.9 ± 0.7 kcal/mol). This

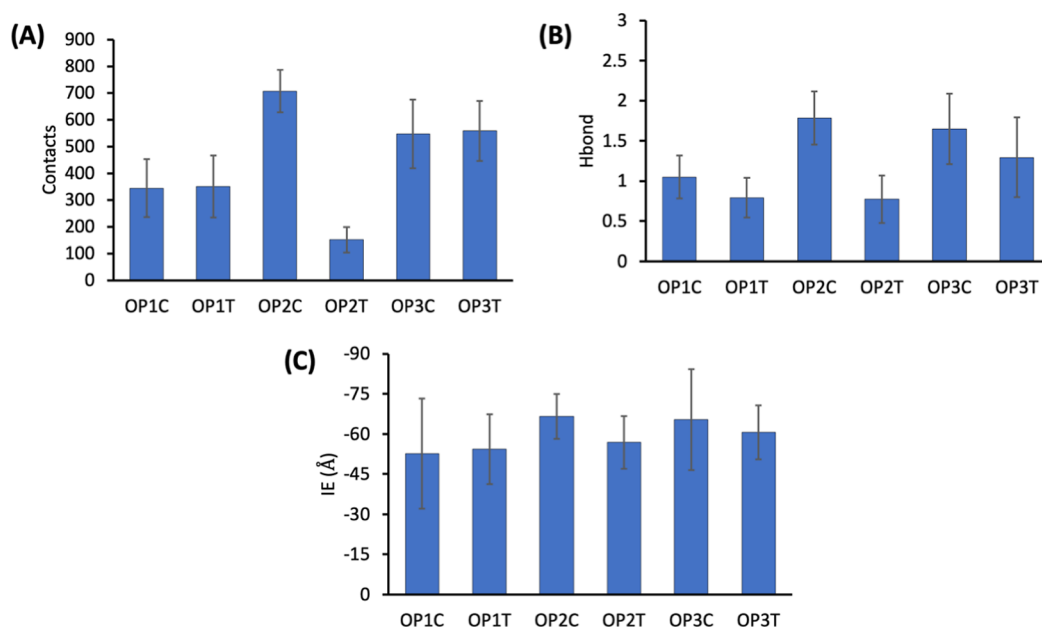


Figure 5. (A) The calculated number of contacts between different antagonists and β_2 -AR (5 Å cutoff distance). (B) The average number of hydrogen bonds between ligands and the receptor during the simulation. (C) The average interaction energy (IE) between the ligand and β_2 -AR.

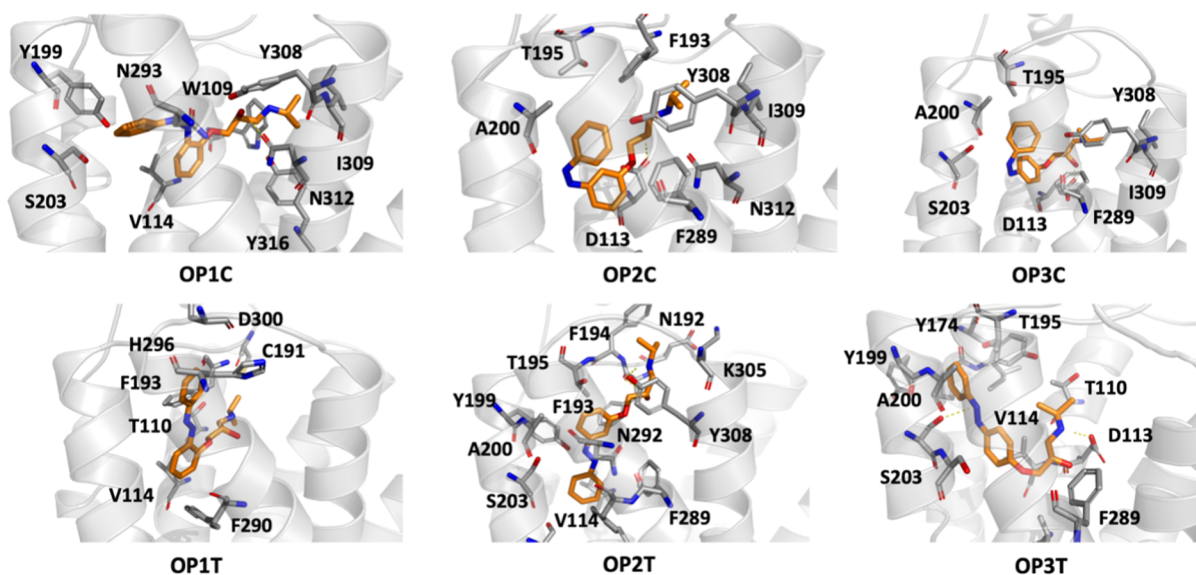


Figure 6. Binding poses for the photoswitchable antagonists (OPs, *cis* and *trans*) in this study. The profiles indicate that the isomeric form of the photoswitchable antagonist plays a crucial role in its interactions with the β_2 -AR. The most representative binding pose obtained from the clustering analysis is shown for each compound.

confirms that the TI simulations accurately capture the critical role of PHE289 in differentiating the binding affinities of the two isomers.

Molecular Interactions between β_2 -AR Complexes with Different Antagonists

To better understand the role of substituents and the isomers (*cis* and *trans*) of the antagonists in their affinity with β_2 -AR, we examined the interaction between β_2 -AR with the three OPs in unbiased production MD simulations ($\sim 1.1 \mu\text{s}$ for each compound). Key results are discussed here, and a more detailed discussion of the protein dynamics and the protein–ligand interactions at the level of individual amino acid residues is provided in the [Supporting Information](#).

The number of contacts between the drugs and the receptor often serves as a useful metric for qualitatively comparing binding affinity. A higher number of contacts generally corresponds to stronger molecular interactions and higher binding affinity. As shown in [Figure 5A](#), the ligand's isomeric form plays a key role in its interaction with β_2 -AR. For example, the OP2C \rightarrow OP2T isomerization can diminish the binding affinity by 1 ± 1 kcal/mol, as predicted by Approach A of the TI method ([Table 1](#)). Consistent with the free energy calculations, the OP2C exhibits the highest number of contacts (707 ± 80), indicating strong interaction with β_2 -AR. In contrast, OP2T demonstrates the lowest number of contacts (152 ± 48), suggesting a weaker interaction. This result is also consistent with the clustering analysis.

The hydrogen bonds (H-bonds) between protein and ligand are one of the most important binding interactions. The calculated average number of H-bonds between β_2 -AR and the ligand is presented in Figure 5B. OP2C forms the largest number of H-bond interactions with β_2 -AR among all OPs in all isomeric forms, consistent with its highest binding affinity. Moreover, the H-bond analysis highlights the role of the isomeric form in light-responsive binding affinity differences. Based on protein–ligand contact profiles (Figure 6), the hydroxyl group of the side chain of OP2C participates in considerable polar interactions with the binding pocket, especially the electrostatic and hydrogen bond interactions with ASP113, ASN 312, and SER207 residues. In addition, the azobenzene moiety of OP2C has hydrophobic interactions with the PHE193, PHE289, ALA200, TYR308, and ILE309 residues, which stabilize OP2C inside the binding pocket. In contrast, for OP2T, its side chain forms a hydrogen bond with the PHE193 residue, instead of a hydrophobic interaction as observed with OP2C. Moreover, the azobenzene moiety of OP2T has fewer polar interactions with the ASP113 and ASN312 residues, as well as fewer contacts with these hydrophobic residues. Its azobenzene moiety also has partial contact with the Y199 residue, but without forming stable hydrogen bonds or π – π interactions between their aromatic rings.

In contrast to OP2C, the side chain of OP1C does not participate in strong electrostatic interactions with ASP113 and instead interacts with this residue primarily through less stable van der Waals contacts, diminishing their binding interactions, consistent with the OP1C→OP2C TI result and experimental data (Table 2). For the OP3, a clear isomer-dependent behavior is observed: the OP3C forms two stable H-bonds with ASP113 and ASN312, whereas the OP3T forms only a single H-bond with ASP113. The reduced electrostatic interactions in the OP3T than the OP3C is consistent with the *cis*-to-*trans* TI results and experimental data (Table 1).

Our analysis is in qualitative agreement with the trends observed in previous site-directed mutagenesis experiments of the OP2(S),³² and provides additional atomistic-level insight into the origin of the isomer-dependent binding affinity. In the 1.1 μ s unbiased MD simulations, the *cis* isomer OP2C adopts a binding pose that allows its hydroxyl group to engage in strong polar interactions with conserved residues such as ASP113 and ASN312, while its aromatic moiety penetrates deeply into the hydrophobic pocket and form strong van der Waals interactions with the nonpolar residues such as PHE193 and PHE289. These interaction patterns observed in the simulation are consistent with the mutagenesis experiments,³² which showed that the N312Q and F289A mutations lead to a considerable reduction in the binding affinity of the *cis* isomer, confirming the critical role of this residue in the binding of OP2C.

In contrast, the *trans* isomer OP2T fails to penetrate deeply into the binding pocket, and has fewer hydrogen bonding and less favorable van der Waals interactions with the protein, thereby reducing its binding stability compared to OP2C. This is consistent with the mutagenesis data showing that replacement of the aromatic residues TYR199 and PHE290 with alanine increases the binding affinity of the OP2T, indicating that the elongated *trans* azobenzene moiety may have some extent of steric clashes with these residues. Moreover, our observation that OP2T forms weaker polar interactions with ASP113 and ASN312 directly supports the

experimental conclusion that the *trans* configuration disrupts the critical H-bond interaction network required for high-affinity binding.

Overall, the MD simulation and TI results validate the experimental mutagenesis data³² and confirm the proposed molecular mechanism underlying the isomer-dependent binding behavior. The *cis* isomer adopts a bent binding pose that allows more favorable interactions with both polar and hydrophobic residues within the β_2 -AR binding pocket, leading to a stronger binding affinity than the *trans* isomer.

To further quantify the effects of isomers and substituents on the strength of protein–ligand interactions, we analyzed the average interaction energy (IE) between the OPs with the β_2 -AR (Figure 5C), taking into account both van der Waals and electrostatic interactions. The trend of calculated IE values aligns well with the trends of binding affinities from experiments and free energy calculations (TI, WT-MTD, and US, Table 1), i.e., OP1T > OP1C, OP2C > OP2T, and OP3C > OP3T.⁷ Additionally, the IEs reveal that OP2C exhibits the highest binding affinity among all OPs, consistent with H-bonds and contact number analysis. Our results demonstrate a considerable linear correlation between the calculated number of H-bonds and interaction energy. As shown in Figure S8, an increase in H-bond interactions between the antagonists and β_2 -AR correlates well with an increase in the magnitude of IE. This finding underscores the critical role of H-bonds in the binding interactions between the antagonist and the β_2 -AR.

Overall, these results suggest that OP2C is the most effective antagonist against β_2 -AR compared to the other compounds, in agreement with the experiments and free energy calculations. This is due to its strongest interactions (H-bond, electrostatic, and van der Waals) with β_2 -AR, which is consistent with the highest number of contacts.

Discussions on the Methodological Details of Free Energy Simulations

For consistent comparisons across the different free energy methods, the same atomic charge set derived for the *cis* isomer was used for both the *cis* and *trans* isomers in the TI calculations for Approaches A and B. This is because in the US and WT-MTD simulations, the isomerization process was modeled by biasing the torsional modes while keeping the point charges unchanged. Although in principle the two isomers may exhibit different charge distributions, in practice, separate charge models were not introduced for each isomer of each compound. In our preliminary tests at the early stage of this study, such a constraint on the force field parameters, to some extent, helps avoid overfitting issues and ensures model robustness, while enabling direct comparability across different computational methods.

It is also worth noting that the *cis* ↔ *trans* isomerization of these ligands can result in protein structural changes, which usually take time to fully relax in free energy calculations. However, we emphasize that the ligands under study were all designed as antagonists of β -ARs, and their binding to the receptors stabilizes the inactive state of the otherwise apo receptor (Figure S7), rather than inducing large conformational changes from the inactive to the active state, which is required for downstream signaling. The role of ligand isomerization is thus mainly to modulate ligand-binding affinity rather than to cause significant conformational changes of the receptors. This claim is also supported by the inhibitory

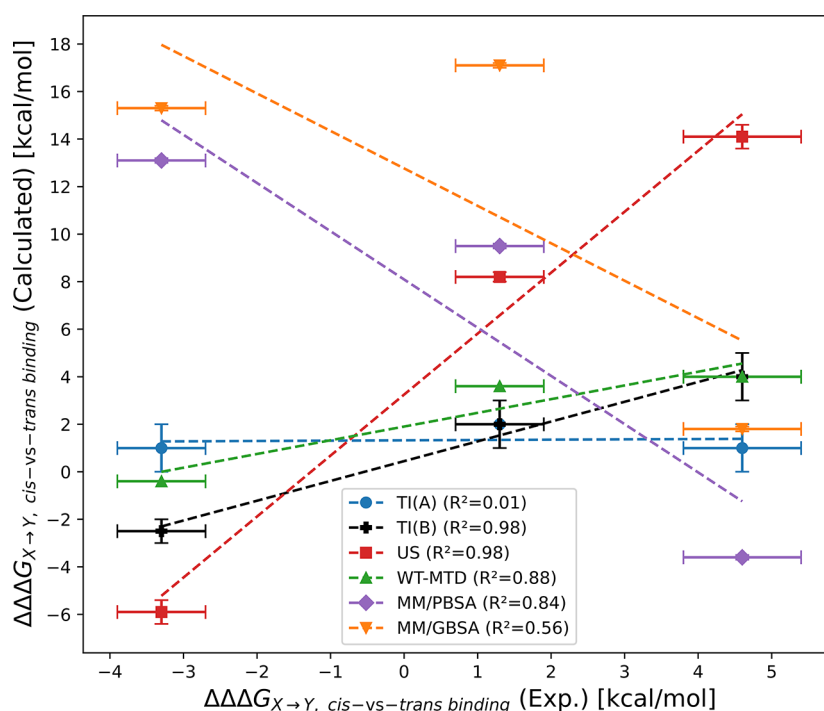


Figure 7. Comparison of experimental and calculated $\Delta\Delta\Delta G_{X \rightarrow Y, cis-vs-trans\ binding}$ values across different computational approaches for the transitions among the three OP ligands. The experimental values are plotted against the corresponding calculated results obtained from TI approach A (TI(A)), TI approach B (TI(B)), US, WT-MTD, MM/PBSA, and MM/GBSA methods. The TI approach B has the best performance in terms of quantitatively reproducing experimental trends in the substituent's effect on the *cis-vs-trans* affinity differential. The US method can provide qualitatively correct predictions but overestimates the magnitudes of the experimental $\Delta\Delta\Delta G$ values.

effect of both isomer forms of each compound in the experimental assays,⁷ even for the less active isomer form.

We also note that, in principle, with ergodic sampling, all free energy methods should converge to the same prediction. However, in practice, it is very difficult to achieve. This is exactly what motivates us to provide pragmatic guidance on which free energy method performs best with finite, affordable sampling in the current study. We reason that approach B of TI is most robust among all tested approaches, as it avoids directly sampling the isomerization event during the alchemical transformation. Approach A of TI, US, and WT-MTD are all based on *cis*↔*trans* isomerization, which is coupled to local changes in the protein binding pocket and takes time to relax, making it more difficult to converge the free energy differences to the ground truth within finite simulation times.

In Figure 7, the performance of the different computational methods is summarized and compared. It presents a direct comparison of the experimental and calculated $\Delta\Delta\Delta G_{X \rightarrow Y, cis-vs-trans\ binding}$ values across all approaches, highlighting the best performance of the TI approach B for quantitatively predicting how substituents influence the light-responsive affinity differential. The US provides the next-best performance in qualitatively capturing these effects. However, as shown by the computational costs summarized in Table S6, both methods require substantial computational resources and are relatively expensive to apply.

CONCLUSION

Quantitatively predicting the light-responsive bioactivity of photoswitchable ligands targeting biomolecules is a crucial goal in photopharmacology. However, a lack of systematic benchmarking of existing free energy methods for this task,

especially in the challenging cases of membrane proteins, hinders the development of accurate computational design platforms. To this end, we benchmarked the accuracy of several widely used free energy methods (TI, MTD, US, MM/PBSA, and MM/GBSA) against experiments for quantifying the light-responsive affinity differential of a series of photo-switchable antagonists targeting β_1 -AR and β_2 -AR.

Our calculations indicate that the compound-to-compound TI method (Approach B) has the best quantitative accuracy in predicting the impacts of chemical modifications on the *cis-vs-trans* affinity differential, as well as on the binding selectivity between receptor subtypes (β_1 -AR and β_2 -AR). Achieving both tasks is essential for maximizing light-responsiveness in bioactivity and reducing off-target toxicity. The second task is especially important for the photopharmacology of GPCRs, where different receptor subtypes initiating distinct signaling processes coexist in the cell membrane. As another remarkable result, this TI method correctly predicts that removing the *p*-acetamido group from PLZ2 and fine-tuning its chirality, which yields the OP2(S), can significantly enhance the “*cis*-on” effect. This was regarded as a key achievement in the experimental design campaigns of the OPs.^{7,32} The only drawback of this TI method is that it does not directly estimate the *cis-vs-trans* affinity differential of an individual ligand, i.e., whether the compound exhibits the “*cis*-on” or “*trans*-on” effect, and its magnitude. For this purpose, as a complementary approach, the *cis*-to-*trans* TI method, which alchemically converts between the two isomeric forms of the same ligand, can be used with acceptable accuracy.

Second to the compound-to-compound TI, the US method can qualitatively capture the trend of the *cis-vs-trans* affinity differential across the three OPs, as well as the active isomer

form for each ligand. However, it significantly overestimates the magnitudes of light-responsive affinity differential, as well as the substituents' effects on it. Thus, this method is suitable for qualitative trend prediction instead of quantitative characterization of the "cis-on" or "trans-on" effects. Moreover, the WT-MTD method, similar to the US method, can capture the experimental trend, but the application of this approach is faced with challenges in achieving convergence due to unstable ligand binding during the simulations. We note that WT-MTD has been successfully applied to estimating the *cis*-vs-*trans* affinity differential of photoswitchable inhibitors in tubulin.¹⁶ However, during these simulations, external biasing potentials were employed to restrain the ligand in the binding pocket. This is consistent with our observation in the simulation of OPs in β_2 -AR.¹⁶

The MM/PBSA and MM/GBSA methods have the worst performance among all methods tested, perhaps due to the lack of explicit sampling of solvent degrees of freedom. Neither method can reliably predict the substituent's effects on the *cis*-vs-*trans* affinity differential, or even whether a ligand has the "cis-on" effect, the latter of which being a much simpler task. These methods also have poor performance for the photo-statin-tubulin system, as reported in our recent study.¹⁸ Thus, we recommend against using these approaches for the design of photoswitchable ligands targeting biomolecular systems.

Our unbiased MD simulations also reveal that among all OPs, the *cis* isomer of OP2 (OP2C) has the highest binding affinity with β_2 -AR due to forming the largest number of hydrogen bonds and contacts with the protein, consistent with the experiment. Furthermore, adding a *p*-acetamido group to OPs reduced the substituents' effects on the *cis*-vs-*trans* affinity differential. This interesting finding reveals the nontrivial coupling effects between different functional groups that collectively fine-tune the light-responsive bioactivity, which can also be correctly predicted by the compound-to-compound TI method.

It is worth mentioning that although photoswitchable ligands offer a unique opportunity to control drug activity with high spatial and temporal precision, translating these systems into real drugs remains challenging. In practice, photoisomerization rarely produces a single active or inactive isomer, and mixtures of isomers can complicate biological responses.⁸⁷ In addition, both isomers may differ in permeability, metabolism, and off-target interactions, meaning that pharmacokinetics and pharmacodynamics should be considered separately for each state. The chemical and photochemical stability of common photoswitches, particularly azo-based systems, is another concern. Finally, clinical application requires reliable light delivery and careful balance between absorption wavelength, isomerization kinetics and quantum yields, target binding interactions *in vivo*.⁸⁸ Together, these factors highlight both the strong therapeutic promise of photoswitchable ligands and the need for continued optimization to address their pharmacological and translational limitations.

Overall, these results not only enhance our understanding of how photoswitchable ligands enable photocontrol over β -ARs, but also establish a robust computational framework for designing photoswitchable drugs with maximal light-responsiveness in bioactivity and subtype-selectivity. The considerable precision of TI methods, complemented by US for trend validation, is a powerful combination of computational tools for advancing the photopharmacology of membrane receptors.

By quantitatively reproducing experimental light-responsive affinity differentials, the substituent and enantiospecific effects,^{7,32} and by qualitatively interpreting the mutagenesis data,³² this work establishes a strong connection between experiment and predictive molecular simulation for the advancement of GPCR photopharmacology.

■ ASSOCIATED CONTENT

Data Availability Statement

We refer the readers to the Supporting Information file for additional data related to the properties of the molecular systems investigated in this manuscript.

SI Supporting Information

The Supporting Information is available free of charge at <https://pubs.acs.org/doi/10.1021/acs.jmedchem.5c03756>.

Tables S1–S6, the details of free energy changes calculated by TI, US, WT-MTD, and MM/PBSA-(GBSA) methods, and the computational cost; Figures S1–S8, the structure of *cis* OP2 in the vacuum optimized, and the relaxed scans of the ground-state PES of OP2, the initial structure of β_1 -AR used for the MD simulation setup, the potential of mean forces (PMFs) for the ground-state *cis*-to-*trans* isomerization of OP2(S) and OP2(R), the 2D PMFs of *cis*-to-*trans* isomerization calculated using WT-MTD, the 1D PMFs of the ground-state *trans*-to-*cis* isomerization as a function of CV1, the time evolution of the free energy difference, protein–ligand interactions between β_2 -AR and different antagonists, the calculated root-mean square fluctuation (RMSF) for the β_2 -AR, the positive correlation between the average number of H-bonds and the calculated interaction energy (PDF)

The simulation setups of β_1 -AR and β_2 -AR complexes with OP compounds, the script and input files of MD simulations, MM-PB/GB-SA, WT-MTD, US, and TI (ZIP)

■ AUTHOR INFORMATION

Corresponding Author

Ruibin Liang – Department of Chemistry and Biochemistry, Texas Tech University, Lubbock, Texas 79409, United States; orcid.org/0000-0001-8741-1520; Email: rliang@ttu.edu

Authors

Mohammad Khavani – Department of Chemistry and Biochemistry, Texas Tech University, Lubbock, Texas 79409, United States

Amirhossein Bakhtiari – Department of Chemistry and Biochemistry, Texas Tech University, Lubbock, Texas 79409, United States

Laleh Khalvati – Department of Chemistry and Biochemistry, Texas Tech University, Lubbock, Texas 79409, United States

Rob Leurs – Division of Medicinal Chemistry, Amsterdam Institute of Molecular and Life Sciences, Faculty of Science, Vrije Universiteit Amsterdam, 1081 HZ Amsterdam, Netherlands; orcid.org/0000-0003-1354-2848

Complete contact information is available at: <https://pubs.acs.org/doi/10.1021/acs.jmedchem.5c03756>

Author Contributions

Ruibin Liang and Rob Leurs conceptualized and designed the research project. Mohammad Khavani, Amirhossein Bakhtiiari, and Laleh Khalvati performed the simulations and analyzed the data. Ruibin Liang, Rob Leurs, Mohammad Khavani, Amirhossein Bakhtiiari, and Laleh Khalvati wrote and revised the manuscript.

Notes

The authors declare no competing financial interest.

ACKNOWLEDGMENTS

This work was supported by the National Institutes of Health (grant number: R35GM150780) and the Texas University Fund (TUF) for the Human Molecular Aging Center at Texas Tech University under internal award #TUF6656. We also acknowledge the computing facilities provided by the High-Performance Computing Center at Texas Tech University.

ABBREVIATIONS

β -ARs	beta-adrenergic receptors
CV	collective variable
GPCR	G-protein-coupled receptor
MM/GBSA	molecular mechanics/generalized Born surface area
MM/PBSA	molecular mechanics/Poisson–Boltzmann surface area
OP	opto-prop
PLZ	photoazolol
QM PES	quantum mechanics potential energy surface
TI	thermodynamic integration
US	umbrella sampling
WT-MTD	well-tempered metadynamics

REFERENCES

- (1) Szymański, W.; Beierle, J. M.; Kistemaker, H. A. V.; Velema, W. A.; Feringa, B. L. Reversible Photocontrol of Biological Systems by the Incorporation of Molecular Photoswitches. *Chem. Rev.* **2013**, *113* (8), 6114–6178.
- (2) Broichhagen, J.; Frank, J. A.; Trauner, D. A Roadmap to Success in Photopharmacology. *Acc. Chem. Res.* **2015**, *48* (7), 1947–1960.
- (3) Hüll, K.; Morstein, J.; Trauner, D. In Vivo Photopharmacology. *Chem. Rev.* **2018**, *118* (21), 10710–10747.
- (4) Kobauri, P.; Dekker, F. J.; Szymanski, W.; Feringa, B. L. Rational Design in Photopharmacology with Molecular Photoswitches. *Angew. Chem. Int.* **2023**, *62* (30), No. e202300681.
- (5) Wijtmans, M.; Josimovic, I.; Vischer, H. F.; Leurs, R. Optical control of Class A G protein-coupled receptors with photoswitchable ligands. *Curr. Opin. Pharmacol.* **2022**, *63*, 102192.
- (6) Brechun, K. E.; Arndt, K. M.; Woolley, G. A. Strategies for the photo-control of endogenous protein activity. *Curr. Opin. Struct. Biol.* **2017**, *45*, 53–58.
- (7) Bosma, R.; Dijon, N. C.; Zheng, Y.; Schihada, H.; Hauwert, N. J.; Shi, S.; Arimont, M.; Riemens, R.; Custers, H.; van de Stolpe, A.; et al. Optical control of the β 2-adrenergic receptor with opto-prop-2: A cis-active azobenzene analog of propranolol. *iScience* **2022**, *25* (9), 104882.
- (8) Gómez-Santacana, X.; Panarello, S.; Rovira, X.; Llebaria, A. Photoswitchable allosteric modulators for metabotropic glutamate receptors. *Curr. Opin. Pharmacol.* **2022**, *66*, 102266.
- (9) Donthamsetti, P.; Winter, N.; Hoagland, A.; Stanley, C.; Visel, M.; Lammel, S.; Trauner, D.; Isacoff, E. Cell specific photoswitchable agonist for reversible control of endogenous dopamine receptors. *Nat. Commun.* **2021**, *12* (1), 4775.

(10) Borowiak, M.; Nahaboo, W.; Reynders, M.; Nekolla, K.; Jalinot, P.; Hasserodt, J.; Rehberg, M.; Delattre, M.; Zahler, S.; Vollmar, A.; et al. Photoswitchable Inhibitors of Microtubule Dynamics Optically Control Mitosis and Cell Death. *Cell* **2015**, *162* (2), 403–411.

(11) Tochitsky, I.; Kienzler, M. A.; Isacoff, E.; Kramer, R. H. Restoring Vision to the Blind with Chemical Photoswitches. *Chem. Rev.* **2018**, *118* (21), 10748–10773.

(12) Kobauri, P.; Galenkamp, N. S.; Schulte, A. M.; de Vries, J.; Simeth, N. A.; Maglia, G.; Thallmair, S.; Kolarski, D.; Szymanski, W.; Feringa, B. L. Hypothesis-Driven, Structure-Based Design in Photopharmacology: The Case of eDHFR Inhibitors. *J. Med. Chem.* **2022**, *65* (6), 4798–4817.

(13) Papadourakis, M.; Sinenka, H.; Matricon, P.; Hénin, J.; Brannigan, G.; Pérez-Benito, L.; Pande, V.; van Vlijmen, H.; de Graaf, C.; Deflorian, F.; et al. Alchemical free energy calculations on membrane-associated proteins. *J. Chem. Theory Comput.* **2023**, *19* (21), 7437–7458.

(14) Rastogi, S. K.; Zhao, Z.; Barrett, S. L.; Shelton, S. D.; Zafferani, M.; Anderson, H. E.; Blumenthal, M. O.; Jones, L. R.; Wang, L.; Li, X.; et al. Photoresponsive azo-combretastatin A-4 analogues. *Eur. J. Med. Chem.* **2018**, *143*, 1–7.

(15) Axelrod, S.; Shakhnovich, E.; Gómez-Bombarelli, R. Mapping the Space of Photoswitchable Ligands and Photodrugable Proteins with Computational Modeling. *J. Chem. Inf. Model.* **2023**, *63* (18), 5794–5802.

(16) Wranik, M.; Weinert, T.; Slavov, C.; Masini, T.; Furrer, A.; Gaillard, N.; Gioia, D.; Ferrarotti, M.; James, D.; Glover, H.; et al. Watching the release of a photopharmacological drug from tubulin using time-resolved serial crystallography. *Nat. Commun.* **2023**, *14* (1), 903.

(17) Gaspari, R.; Prota, A. E.; Bargsten, K.; Cavalli, A.; Steinmetz, M. O. Structural basis of cis- and trans-combretastatin binding to tubulin. *Chem* **2017**, *2* (1), 102–113.

(18) Bakhtiiari, A.; Khavani, M.; Costa, G. J.; Liang, R. A Multiscale Simulation Framework for Elucidating Photochemical Structure–Activity Relationships of Photoswitchable Ligands in Complex Biomolecular Environments. *J. Chem. Inf. Model.* **2025**, *65*, 12861.

(19) Christ, C. D.; Fox, T. Accuracy assessment and automation of free energy calculations for drug design. *J. Chem. Inf. Model.* **2014**, *54* (1), 108–120.

(20) Darve, E. Thermodynamic Integration Using Constrained and Unconstrained Dynamics. In *Free Energy Calculations: Theory and Applications in Chemistry and Biology*; Chipot, C., Pohorille, A., Eds.; Springer Berlin Heidelberg, 2007; pp 119–170.

(21) Homeyer, N.; Stoll, F.; Hillisch, A.; Gohlke, H. Binding free energy calculations for lead optimization: assessment of their accuracy in an industrial drug design context. *J. Chem. Theory Comput.* **2014**, *10* (8), 3331–3344.

(22) Wojtas-Niziurski, W.; Meng, Y.; Roux, B. t.; Bernèche, S. Self-learning adaptive umbrella sampling method for the determination of free energy landscapes in multiple dimensions. *J. Chem. Theory Comput.* **2013**, *9* (4), 1885–1895.

(23) Kastner, J. Umbrella sampling. *Wiley Interdiscip. Rev. Comput. Mol. Sci.* **2011**, *1* (6), 932–942.

(24) You, W.; Tang, Z.; Chang, C.-E. A. Potential mean force from umbrella sampling simulations: what can we learn and what is missed? *J. Chem. Theory Comput.* **2019**, *15* (4), 2433–2443.

(25) Bussi, G.; Laio, A. Using metadynamics to explore complex free-energy landscapes. *Nat. Rev. Phys.* **2020**, *2* (4), 200–212.

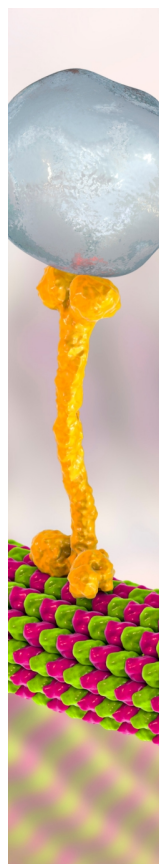
(26) Cavalli, A.; Spitaleri, A.; Saladino, G.; Gervasio, F. L. Investigating drug–target association and dissociation mechanisms using metadynamics-based algorithms. *Acc. Chem. Res.* **2015**, *48* (2), 277–285.

(27) Barducci, A.; Bussi, G.; Parrinello, M. Well-Tempered Metadynamics: A Smoothly Converging and Tunable Free-Energy Method. *Phys. Rev. Lett.* **2008**, *100* (2), 020603.

(28) Laio, A.; Parrinello, M. Escaping free-energy minima. *Proc. Natl. Acad. Sci. U.S.A.* **2002**, *99* (20), 12562–12566.

- (29) Wang, E.; Sun, H.; Wang, J.; Wang, Z.; Liu, H.; Zhang, J. Z.; Hou, T. End-point binding free energy calculation with MM/PBSA and MM/GBSA: strategies and applications in drug design. *Chem. Rev.* **2019**, *119* (16), 9478–9508.
- (30) Srivastava, H. K.; Sastry, G. N. Molecular dynamics investigation on a series of HIV protease inhibitors: assessing the performance of MM-PBSA and MM-GBSA approaches. *J. Chem. Inf. Model.* **2012**, *52* (11), 3088–3098.
- (31) Duran-Corbera, A.; Catena, J.; Otero-Viñas, M.; Llebaria, A.; Rovira, X. Photoswitchable Antagonists for a Precise Spatiotemporal Control of β 2-Adrenoceptors. *J. Med. Chem.* **2020**, *63* (15), 8458–8470.
- (32) Shi, S.; Zheng, Y.; Goulding, J.; Marri, S.; Lucarini, L.; Konecny, B.; Sgambellone, S.; Villano, S.; Bosma, R.; Wijtmans, M.; et al. A high-affinity, cis-on photoswitchable beta blocker to optically control β 2-adrenergic receptors in vitro and in vivo. *Biochem. Pharmacol.* **2024**, *226*, 116396.
- (33) Rosenbaum, D. M.; Rasmussen, S. G.; Kobilka, B. K. The structure and function of G-protein-coupled receptors. *Nature* **2009**, *459* (7245), 356–363.
- (34) Ricart-Ortega, M.; Font, J.; Llebaria, A. GPCR photopharmacology. *Mol. Cell. Endocrinol.* **2019**, *488*, 36–51.
- (35) Binkhorst, L. C. P.; Josimovic, I.; De Boer, B.; Simon, I. A.; Van Der Aa, F.; Zarzycka, B. A.; De Esch, I. J. P.; Vischer, H. F.; Windhorst, A. D.; Wijtmans, M.; et al. A Radiolabeled Photoswitchable G Protein-Coupled Receptor Antagonist Enlightens Ligand Binding Kinetics Associated with Photoswitching. *J. Am. Chem. Soc.* **2025**, *147* (27), 23991–24000.
- (36) Cao, Y.; Shi, S.; Does, S. A. H.; Buzink, C. M. L.; Gao, M.; de Esch, I. J. P.; Vischer, H. F.; Wijtmans, M.; Leurs, R. Photoclenbuterol: Optical Control of β 2-Adrenergic Receptor Signaling by Photoswitchable Ligand Efficacy. *J. Med. Chem.* **2025**, *68*, 12911.
- (37) Donthamsetti, P.; Konrad, D. B.; Hetzler, B.; Fu, Z.; Trauner, D.; Isacoff, E. Y. Selective Photoswitchable Allosteric Agonist of a G Protein-Coupled Receptor. *J. Am. Chem. Soc.* **2021**, *143* (24), 8951–8956.
- (38) Donthamsetti, P. C.; Broichhagen, J.; Vyklicky, V.; Stanley, C.; Fu, Z.; Visel, M.; Levitz, J. L.; Javitch, J. A.; Trauner, D.; Isacoff, E. Y. Genetically Targeted Optical Control of an Endogenous G Protein-Coupled Receptor. *J. Am. Chem. Soc.* **2019**, *141* (29), 11522–11530.
- (39) Donthamsetti, P. C.; Winter, N.; Schönberger, M.; Levitz, J.; Stanley, C.; Javitch, J. A.; Isacoff, E. Y.; Trauner, D. Optical Control of Dopamine Receptors Using a Photoswitchable Tethered Inverse Agonist. *J. Am. Chem. Soc.* **2017**, *139* (51), 18522–18535.
- (40) Levitz, J.; Broichhagen, J.; Leippe, P.; Konrad, D.; Trauner, D.; Isacoff, E. Y. Dual optical control and mechanistic insights into photoswitchable group II and III metabotropic glutamate receptors. *Proc. Natl. Acad. Sci. U.S.A.* **2017**, *114* (17), E3546–E3554.
- (41) Duran-Corbera, A.; Faria, M.; Ma, Y.; Prats, E.; Dias, A.; Catena, J.; Martinez, K. L.; Raldua, D.; Llebaria, A.; Rovira, X. A Photoswitchable Ligand Targeting the β 1-Adrenoceptor Enables Light-Control of the Cardiac Rhythm. *Angew. Chem. Int. Ed.* **2022**, *61* (30), No. e202203449.
- (42) Lefkowitz, R. J. Seven transmembrane receptors—A brief personal retrospective. *Biochim. Biophys. Acta Biomembr.* **2007**, *1768* (4), 748–755.
- (43) Lefkowitz, R. J. The superfamily of heptahelical receptors. *Nat. Cell Biol.* **2000**, *2* (7), E133–E136.
- (44) Seddon, A. M.; Curnow, P.; Booth, P. J. Membrane proteins, lipids and detergents: not just a soap opera. *Biochim. Biophys. Acta Biomembr.* **2004**, *1666* (1–2), 105–117.
- (45) Kobilka, B. The structural basis of G-protein-coupled receptor signaling (Nobel Lecture). *Angew. Chem. Int. Ed. Engl.* **2013**, *52* (25), 6380.
- (46) Santos, R.; Ursu, O.; Gaulton, A.; Bento, A. P.; Donadi, R. S.; Bologa, C. G.; Karlsson, A.; Al-Lazikani, B.; Hersey, A.; Oprea, T. I.; et al. A comprehensive map of molecular drug targets. *Nat. Rev. Drug Discovery* **2017**, *16* (1), 19–34.
- (47) Brooks, A. M.; Gillies, W. Ocular β -blockers in glaucoma management: clinical pharmacological aspects. *Drugs Aging* **1992**, *2*, 208–221.
- (48) Weis, W. I.; Kobilka, B. K. The molecular basis of G protein-coupled receptor activation. *Annu. Rev. Biochem.* **2018**, *87* (1), 897–919.
- (49) Najafi, A.; Sequeira, V.; Kuster, D. W.; van der Velden, J. β -adrenergic receptor signalling and its functional consequences in the diseased heart. *Eur. J. Clin. Invest.* **2016**, *46* (4), 362–374.
- (50) Barnes, P. J. Biochemical basis of asthma therapy. *J. Biol. Chem.* **2011**, *286* (38), 32899–32905.
- (51) Baker, J. G. The selectivity of β -adrenoceptor antagonists at the human β 1, β 2 and β 3 adrenoceptors. *Br. J. Pharmacol.* **2005**, *144* (3), 317–322.
- (52) Uhlén, M.; Fagerberg, L.; Hallström, B. M.; Lindskog, C.; Oksvold, P.; Mardinoglu, A.; Sivertsson, Å.; Kampf, C.; Sjöstedt, E.; Asplund, A.; et al. Tissue-based map of the human proteome. *Science* **2015**, *347* (6220), 1260419.
- (53) Filippi, L.; Dal Monte, M.; Casini, G.; Daniotti, M.; Sereni, F.; Bagnoli, P. Infantile hemangiomas, retinopathy of prematurity and cancer: a common pathogenetic role of the β -adrenergic system. *Med. Res. Rev.* **2015**, *35* (3), 619–652.
- (54) Ishchenko, A.; Stauch, B.; Han, G. W.; Batyuk, A.; Shiriaeva, A.; Li, C.; Zatssep, N.; Weierstall, U.; Liu, W.; Nango, E.; et al. Toward G protein-coupled receptor structure-based drug design using X-ray lasers. *IUCrJ* **2019**, *6* (6), 1106–1119.
- (55) Manna, M.; Kulig, W.; Javanainen, M.; Tynkkynen, J.; Hensen, U.; Müller, D. J.; Rog, T.; Vattulainen, I. How to minimize artifacts in atomistic simulations of membrane proteins, whose crystal structure is heavily engineered: β 2-adrenergic receptor in the spotlight. *J. Chem. Theory Comput.* **2015**, *11* (7), 3432–3445.
- (56) Webb, B.; Sali, A. Comparative protein structure modeling using MODELLER. *Curr. Protoc. Bioinform.* **2016**, *86* (1), 1–37.
- (57) Trott, O.; Olson, A. J. AutoDock Vina: improving the speed and accuracy of docking with a new scoring function, efficient optimization, and multithreading. *J. Comput. Chem.* **2010**, *31* (2), 455–461.
- (58) Anandakrishnan, R.; Aguilar, B.; Onufriev, A. V. H++ 3.0: automating p K prediction and the preparation of biomolecular structures for atomistic molecular modeling and simulations. *Nucleic Acids Res.* **2012**, *40* (W1), W537–W541.
- (59) Wu, E. L.; Cheng, X.; Jo, S.; Rui, H.; Song, K. C.; Dávila-Contreras, E. M.; Qi, Y.; Lee, J.; Monje-Galvan, V.; Venable, R. M. CHARMM-GUI Membrane Builder toward Realistic Biological Membrane Simulations; Wiley Online Library, 2014.
- (60) Hanson, M. A.; Cherezov, V.; Griffith, M. T.; Roth, C. B.; Jaakola, V.-P.; Chien, E. Y.; Velasquez, J.; Kuhn, P.; Stevens, R. C. A specific cholesterol binding site is established by the 2.8 Å structure of the human β 2-adrenergic receptor. *Structure* **2008**, *16* (6), 897–905.
- (61) Cherezov, V.; Rosenbaum, D. M.; Hanson, M. A.; Rasmussen, S. G.; Thian, F. S.; Kobilka, T. S.; Choi, H.-J.; Kuhn, P.; Weis, W. I.; Kobilka, B. K.; et al. High-resolution crystal structure of an engineered human β 2-adrenergic G protein-coupled receptor. *Science* **2007**, *318* (5854), 1258–1265.
- (62) Xu, X.; Kaindl, J.; Clark, M. J.; Hübner, H.; Hirata, K.; Sunahara, R. K.; Gmeiner, P.; Kobilka, B. K.; Liu, X. Binding pathway determines norepinephrine selectivity for the human β 1AR over β 2AR. *Cell Res.* **2021**, *31* (5), 569–579.
- (63) Jorgensen, W. L.; Chandrasekhar, J.; Madura, J. D.; Impey, R. W.; Klein, M. L. Comparison of simple potential functions for simulating liquid water. *J. Chem. Phys.* **1983**, *79* (2), 926–935.
- (64) Maier, J. A.; Martinez, C.; Kasavajhala, K.; Wickstrom, L.; Hauser, K. E.; Simmerling, C. ff14SB: improving the accuracy of protein side chain and backbone parameters from ff99SB. *J. Chem. Theory Comput.* **2015**, *11* (8), 3696–3713.
- (65) Skjevik, Å. A.; Madej, B. D.; Dickson, C. J.; Lin, C.; Teigen, K.; Walker, R. C.; Gould, I. R. Simulation of lipid bilayer self-assembly using all-atom lipid force fields. *Phys. Chem. Chem. Phys.* **2016**, *18* (15), 10573–10584.

- (66) Wang, J.; Wolf, R. M.; Caldwell, J. W.; Kollman, P. A.; Case, D. A. Development and testing of a general amber force field. *J. Comput. Chem.* **2004**, *25* (9), 1157–1174.
- (67) Wang, J.; Wang, W.; Kollman, P. A.; Case, D. A. Automatic atom type and bond type perception in molecular mechanical calculations. *J. Mol. Graph. Model.* **2006**, *25* (2), 247–260.
- (68) Liang, R.; Bakhtiari, A. Effects of enzyme–ligand interactions on the photoisomerization of a light-regulated chemotherapeutic drug. *J. Phys. Chem. B* **2022**, *126* (12), 2382–2393.
- (69) Yu, J. K.; Bannwarth, C.; Hohenstein, E. G.; Martínez, T. J. Ab Initio Nonadiabatic Molecular Dynamics with Hole–Hole Tamm–Dancoff Approximated Density Functional Theory. *J. Chem. Theory Comput.* **2020**, *16* (9), 5499–5511.
- (70) Yu, J. K.; Bannwarth, C.; Liang, R.; Hohenstein, E. G.; Martínez, T. J. Nonadiabatic Dynamics Simulation of the Wavelength-Dependent Photochemistry of Azobenzene Excited to the $n\pi^*$ and $\pi\pi^*$ Excited States. *J. Am. Chem. Soc.* **2020**, *142* (49), 20680–20690.
- (71) Liang, R. First-Principles Nonadiabatic Dynamics Simulation of Azobenzene Photodynamics in Solutions. *J. Chem. Theory Comput.* **2021**, *17* (5), 3019–3030.
- (72) Liang, R.; Bakhtiari, A. Multiscale simulation unravels the light-regulated reversible inhibition of dihydrofolate reductase by phototrexate. *J. Chem. Phys.* **2022**, *156* (24), 245102.
- (73) Bakhtiari, A.; Costa, G. J.; Liang, R. On the Simulation of Thermal Isomerization of Molecular Photoswitches in Biological Systems. *J. Chem. Theory Comput.* **2023**, *19* (18), 6484–6499.
- (74) Seritan, S.; Bannwarth, C.; Fales, B. S.; Hohenstein, E. G.; Kokkila-Schumacher, S. I.; Luehr, N.; Snyder, J. W.; Song, C.; Titov, A. V.; Ufimtsev, I. S.; et al. TeraChem: Accelerating electronic structure and ab initio molecular dynamics with graphical processing units. *J. Chem. Phys.* **2020**, *152* (22), 224110.
- (75) Seritan, S.; Bannwarth, C.; Fales, B. S.; Hohenstein, E. G.; Isborn, C. M.; Kokkila-Schumacher, S. I.; Li, X.; Liu, F.; Luehr, N.; Snyder, J. W., Jr; Song, C.; et al. A graphical processing unit-accelerated electronic structure package for large-scale ab initio molecular dynamics. *Wiley Interdiscip. Rev.: Comput. Mol. Sci.* **2021**, *11* (2), No. e1494.
- (76) Uberuaga, B. P.; Anghel, M.; Voter, A. F. Synchronization of trajectories in canonical molecular-dynamics simulations: Observation, explanation, and exploitation. *J. Chem. Phys.* **2004**, *120* (14), 6363–6374.
- (77) Sindhikara, D. J.; Kim, S.; Voter, A. F.; Roitberg, A. E. Bad seeds sprout perilous dynamics: Stochastic thermostat induced trajectory synchronization in biomolecules. *J. Chem. Theory Comput.* **2009**, *5* (6), 1624–1631.
- (78) Darden, T.; York, D.; Pedersen, L. Particle mesh Ewald: An $N \log(N)$ method for Ewald sums in large systems. *J. Chem. Phys.* **1993**, *98*, 10089.
- (79) Ryckaert, J.-P.; Ciccotti, G.; Berendsen, H. J. Numerical integration of the cartesian equations of motion of a system with constraints: molecular dynamics of n-alkanes. *J. Comput. Phys.* **1977**, *23* (3), 327–341.
- (80) Case, D. A.; Aktulga, H. M.; Belfon, K.; Ben-Shalom, I. Y.; Berryman, J. T.; Brozell, S. R.; Cerutti, D. S.; Cheatham III, T. E.; Cisneros, G. A.; Cruzeiro, V. W. D. *Amber 2023*; University of California: San Francisco, 2023.
- (81) He, X.; Liu, S.; Lee, T.-S.; Ji, B.; Man, V. H.; York, D. M.; Wang, J. Fast, accurate, and reliable protocols for routine calculations of protein–ligand binding affinities in drug design projects using AMBER GPU-TI with ff14SB/GAFF. *ACS Omega* **2020**, *5* (9), 4611–4619.
- (82) Kumar, S.; Rosenberg, J. M.; Bouzida, D.; Swendsen, R. H.; Kollman, P. A. The weighted histogram analysis method for free-energy calculations on biomolecules. I. The method. *J. Comput. Chem.* **1992**, *13* (8), 1011–1021.
- (83) Tribello, G. A.; Bonomi, M.; Branduardi, D.; Camilloni, C.; Bussi, G. PLUMED 2: New feathers for an old bird. *Comput. Phys. Commun.* **2014**, *185* (2), 604–613.
- (84) Lu, Q.; Luo, R. A Poisson–Boltzmann dynamics method with nonperiodic boundary condition. *J. Chem. Phys.* **2003**, *119* (21), 11035–11047.
- (85) Miller, B. R., III; McGee, T. D., Jr; Swails, J. M.; Homeyer, N.; Gohlke, H.; Roitberg, A. E. MMPBSA.py: an efficient program for end-state free energy calculations. *J. Chem. Theory Comput.* **2012**, *8* (9), 3314–3321.
- (86) Han, Y.; Dawson, J. R.; DeMarco, K. R.; Rouen, K. C.; Bekker, S.; Yarov-Yarovoy, V.; Clancy, C. E.; Xiang, Y. K.; Vorobyov, I. Elucidation of a dynamic interplay between a beta-2 adrenergic receptor, its agonist, and stimulatory G protein. *Proc. Natl. Acad. Sci. U.S.A.* **2023**, *120* (10), No. e2215916120.
- (87) Fuchter, M. J. On the promise of photopharmacology using photoswitches: a medicinal chemist’s perspective. *J. Med. Chem.* **2020**, *63* (20), 11436–11447.
- (88) Tsai, Y.-H.; Essig, S.; James, J. R.; Lang, K.; Chin, J. W. Selective, rapid and optically switchable regulation of protein function in live mammalian cells. *Nat. Chem.* **2015**, *7* (7), 554–561.



CAS BIOFINDER DISCOVERY PLATFORM™

BRIDGE BIOLOGY AND CHEMISTRY FOR FASTER ANSWERS

Analyze target relationships,
compound effects, and disease
pathways

Explore the platform



A Division of the
American Chemical Society